Measurements and Modeling of DO_2 Formation in the Reactions of C_2D_5 and C_3D_7 Radicals with O_2†

Edgar G. Estupiñán,‡ Jared D. Smith,§ Atsumu Tezaki,|| Stephen J. Klippenstein,⊥ and Craig A. Taatjes*

Combustion Research Facility, Mail Stop 9055, Sandia National Laboratories, Livermore, California 94551-0969

Received: November 15, 2006; In Final Form: January 15, 2007

Time-resolved production of HO_2 and DO_2 from the reactions of nondeuterated and deuterated ethyl and propyl radicals with O_2 are measured as a function of temperature and pressure in the "transition region" between 623 and 748 K using the technique of laser photolysis/long path frequency modulation spectroscopy. Experimental measurements, using both pulsed-photolytic Cl-atom-initiated oxidation of ethane and propane and direct photolysis of ethyl, *n*-propyl, and isopropyl iodides, are compared to kinetic models based on the results of time-dependent master equation calculations with *ab initio* characterization of stationary points. The formation of DO_2 and HO_2 from the subsequent reaction of the alkyl radicals with O_2 is followed by infrared frequency modulation spectroscopy. The concentration of I atoms is simultaneously monitored by direct absorption of a second laser probe on the spin−orbit transition. The kinetic models accurately describe the time scale and amplitude of the DO_2 and HO_2 formation resulting from $C_2D_5 + O_2$, *n*-$C_3D_7 + O_2$, *i*-$C_3D_7 + O_2$, and *i*-$C_3H_7 + O_2$. Overall, a very good level of agreement is found between theory and experiments over a wide range of temperatures, pressures, and O_2 concentrations. Good agreement is also found between previous literature studies and the theory presented in this work except in the case of the high-temperature rate coefficients for the reaction of *i*-$C_3H_7 + O_2$ to form propene. A reinvestigation of the high-temperature kinetics of the *i*-$C_3H_7 + O_2$ reaction appears warranted. The results from the present work suggest that the theory for formation of HO_2 from the reactions of ethyl and both isomeric forms of propyl radicals with O_2 are very well established at this time. It is hoped that these reactions can now form the groundwork for the study and interpretation of larger and more complex $R + O_2$ systems.

Introduction

The reaction between alkyl radicals, R, and molecular oxygen plays a central role in the oxidation mechanism of alkanes at low and moderate temperatures, which naturally has implications on the chemistry of combustion systems and of the atmosphere. In the atmosphere, alkylperoxy radicals (RO_2), which are formed in the initial step of the reaction, are very important intermediates in the troposphere affecting ozone concentrations and its oxidizing capacity.[1−3] In combustion chemistry, $R + O_2$ reactions have received special attention because of the important role they play in autoignition phenomena. The properties of these reactions cause the change in oxidation mechanism of alkanes between approximately 500 and 800 K, which results in the "negative temperature coefficient" (NTC) behavior in hydrocarbon oxidation.

$R + O_2$ reactions proceed via a bound alkylperoxy (RO_2) radical, which can subsequently eliminate HO_2 to form a conjugate alkene or isomerize by intramolecular hydrogen abstraction to form a hydroperoxyalkyl radical (denoted as QOOH). The QOOH radical can in turn react with O_2, which is thought to be responsible for chain branching at low temperature,[4,5] or dissociate to form HO_2 + alkene or OH + cyclic ether products. Branching between OH and HO_2 among these channels is important for chain propagation because of the different reactivities of the two radicals. At low temperatures (i.e., below 500 K), stabilization to the alkylperoxy radical dominates the reaction. At higher temperatures (i.e., above 800 K), thermal dissociation of the alkylperoxy radical becomes fairly rapid and only bimolecular product channels remain. In the intermediate temperature regime (∼500−800 K), often called the transition region, the consumption of alkyl radicals and the formation of products is not describable by a single rate coefficient but is a complicated convolution of stabilization, dissociation, and elimination processes. It is in this temperature regime that the current work is focused especially because the distribution of the various product channels have a very noticeable effect on chain branching and ignition processes.[4,5]

The ultimate goal of this research is to provide a rigorous basis for kinetic modeling of smaller, simpler, and more easily characterized systems that may then be extended to similar larger $R + O_2$ systems. As the complexity of each system increases, characterization of each reaction provides a basis for interpreting the next system until a general representation of $R + O_2$ reactions is accurately achieved. The ethyl (C_2H_5) + O_2 system is the most extensively studied of the alkyl + O_2 reactions both experimentally[6−19] and theoretically.[18−30] The reaction of ethyl

† Part of the special issue "James A. Miller Festschrift".

* Corresponding author. E-mail: cataatj@sandia.gov.

‡ Present address: Osram Sylvania, Inc. 71 Cherry Hill Drive, Beverly, MA 01915.

§ Present address: Chemical Sciences Division, Ernest Orlando Lawrence Berkeley National Laboratory, Berkeley, CA 94720.

|| Permanent address: School of Science and Engineering, University of Toyama, 3190 Gofuku, 930-8555 Toyama, Japan.

⊥ Chemistry Division, Argonne National Laboratory, Argonne, IL 60439.

10.1021/jp067602a CCC: $37.00
Published on Web 02/23/2007

radical with O_2 is considered the "prototype" alkyl + O_2 reaction because of its relative theoretical tractability and because it is the smallest system where alkene formation and isomerization to QOOH are possible. However, initial product formation studies[13,31,32] have revealed that an increase in alkyl radical chain length leads to an increase in the relative importance of the isomerization step to QOOH. As a result, the reaction of the propyl radical, the next simplest alkyl radical, with O_2, is expected to be a much better prototype for general R + O_2 reactions.

Recently, the time dependent production of HO_2 has been measured for several alkyl + O_2 systems.[6,19,33−38] The experimental measurements, using both pulsed-photolytic Cl-atom initiated oxidation of alkanes[6,19,33−37] and direct photolysis of ethyl, *n*-propyl and isopropyl iodides,[38] have been compared to detailed master equation calculations based on *ab initio* characterizations of the potential energy surfaces for the reactions combined with integrated rate equation models that include both radical formation and radical destruction reactions that occur between species present in the experiment.[19,22,23,37,38] The *ab initio* energies were adjusted to produce agreement with the experimental data and with available literature studies. Such a comparison allows validation of the stationary point energies and thereby individual rate coefficients under experimental conditions where simple kinetic models cannot isolate elementary reaction steps,[39] and appears superior[40] to previous qualitative decompositions.[6,33] The models accurately describe the time behavior and amplitude of the HO_2 from C_2H_5 + O_2 and *n*-C_3H_7 + O_2.[19,37,38] However, the models slightly underestimate the prompt HO_2 formation and the slower, secondary production rate for isopropyl + O_2,[38] although the prediction of HO_2 formation in Cl-initiated propane oxidation is improved.[38] The choice of parameters for the isopropyl + O_2 model presented in previous work[38] was partially determined by the existing literature studies[8,41−43] that constrained the scope of possible changes to the theoretical model. The data presented in this work further constrain the models for ethyl, *n*-propyl and isopropyl + O_2.

The measurement of kinetic isotope effects is a well-established and powerful tool for probing reaction mechanisms and can provide additional data to refine the theoretical estimates of the R + O_2 chemistry. Kinetic isotope effects are interpreted within the framework of the Born−Oppenheimer approximation as measurements of how different masses of nuclei affect motion on the same potential surface.[44] Because most energy transfer and energy exchange mechanisms are affected by the density of vibrational states (and hence the frequencies of vibrational motion), kinetic isotope effects are also expected for energy transfer. It is important to point out that the overall kinetic isotope effect is a complex combination of zero point energy effects, variations in the partition functions of the reactants and transition states, and tunneling effects.

In the present work, time-resolved production of HO_2 and DO_2 from the reactions of nondeuterated and deuterated ethyl and propyl radicals with O_2 is measured as a function of temperature and pressure in the "transition region" between 623 and 748 K. Experimental measurements, using both pulsed-photolytic Cl-atom initiated oxidation of ethane and propane and direct photolysis of ethyl, *n*-propyl and isopropyl iodides, are compared, as in previous work,[19,37,38] to kinetic models based on the results of time-dependent master equation calculations with *ab initio* characterization of stationary points. The present investigation extends the scope of the earlier work in several important aspects. First, because the observed kinetic isotope effect is expected to be a convolution of kinetic isotope effects for the stabilization, redissociation, and elimination pathways, results from studies on the deuterated species place additional demands on the theoretical description of the ethyl and propyl + O_2 potential energy surfaces (i.e., especially in the study of the reaction of isopropyl + O_2, where a previous study[38] suggested that further refinement is still necessary). Second, deuterium kinetic isotope effects resulting from comparing the calculated elementary rate coefficients (arising from solutions to time-dependent master equations) of the nondeuterated to the deuterated ethyl and propyl radicals with O_2 are used to gain insight on the accuracy of the theoretical picture (i.e., in terms of expected H-atom motion). Third, this study forms the basis for future studies of partially deuterated species, which are expected to give site-specific information. Fourth, the direct photolysis studies (which add confidence to the Cl-initiated oxidation experiments and unambiguously probe the reaction of each propyl isomer with O_2, as shown in previous work)[38] permit lower O_2 concentrations to be employed in the experimental studies. Use of lower O_2 concentrations enables measurements of the prompt rise time, a quantity that could not be measured in the Cl-initiated experiments because the O_2 concentration had to be sufficiently larger than the Cl_2 concentration so that the O_2 reaction dominated over the R + Cl_2 chain reaction. Experiments conducted with relatively low O_2 concentrations are particularly useful in the study of the isopropyl + O_2 reaction.

Methods

Experiment. The reactions of ethyl (C_2H_5/C_2D_5) and propyl (C_3H_7/C_3D_7) radicals with O_2 are investigated using a modification of the laser photolysis-continuous wave (CW) infrared two-tone frequency-modulation (FM) method employed previously for R + O_2 reactions.[6,19,33−38] Experiments are carried out either by pulsed-photolytic Cl-atom initiated oxidation of deuterated ethane and propane or by direct photolysis of normal-abundance and deuterated ethyl, *n*-propyl and isopropyl iodides. Both experimental systems are discussed in the following two sub-sections.

Cl-Initiated Experiments. The reaction is initiated by pulsed photolysis of Cl_2 at 355 nm, and C_2D_5 or C_3D_7 are generated by subsequent Cl abstraction from C_2D_6 or C_3D_8 respectively. The alkyl radical then reacts with O_2

$$Cl_2 + h\nu\ (355\ nm) \rightarrow 2Cl \quad (1)$$

$$Cl + RD \rightarrow R + DCl \quad (2)$$

$$R + O_2 \rightarrow \text{products} \quad (3)$$

The subsequent time evolution of the DO_2 reaction product is monitored by absorption of a CW infrared probe. The advantage of the above reaction scheme is that the abstraction of a hydrogen atom from the alkane by a Cl atom is nearly thermoneutral,[45] and, thus, the alkyl radical is generated with negligible excitation above thermal energies. One important disadvantage is that the Cl reaction with alkanes is not isomer-specific. For example, whereas only ethyl radicals can be formed in the reaction of Cl atoms with ethane, the reaction of Cl atoms with propane forms both isomers of propyl radicals, i.e., *n*-propyl and isopropyl radicals. Even though in the reaction of Cl with C_3H_8, product branching fractions are relatively well established below about 500 K,[46,47] the only studies of the *n*-C_3D_7 branching fraction resulting from the C_3D_8 + Cl reaction come from high-temperature extrapolations of unpublished studies over the

temperature range of 300 to 575 K.[48] These studies suggest a primary H-atom kinetic isotope effect (k_H^P/k_D^P) of approximately 4 and a secondary H-atom kinetic isotope effect (k_H^S/k_D^S) of about 1.5. Over the temperature range of the $C_3D_7 + O_2$ experiments (623−703 K), this yields an *n*-C_3D_7 branching fraction of about 0.3.

Another advantage of the Cl-initiated reaction scheme is that the relative yield of DO_2 can be determined by comparing the DO_2 signal to a reference system of Cl-initiated methanol oxidation. Reference experiments are carried out under identical photolysis conditions except that C_2D_6 or C_3D_8 are replaced with a nearly equal concentration of CD_3OD, keeping all other experimental conditions equal. This reaction sequence

$$Cl + CD_3OD \rightarrow CD_2OD + DCl \quad \Phi = 100\% \qquad (4)$$

$$CD_2OD + O_2 \rightarrow CD_2O + DO_2 \quad \Phi = 100\% \qquad (5)$$

produces 100% yield of DO_2 as a product over the temperature range of the current experiments.[49] Therefore, because the initial Cl concentration is the same in both systems, the amount of DO_2 produced from the C_2D_5 or $C_3D_7 + O_2$ reaction can be scaled to the 100% conversion of Cl to DO_2 in reactions 4 and 5 by direct comparison of signal strengths. As it is very important for the accuracy of the experiments to keep identical experimental conditions between the CD_2OD/O_2 system (reference signal) and the R/O_2 system, every effort was made to carry out these back to back experiments as quickly as possible. In general, the reference signal changed by less than 10%, although in a few instances the change was as much as 20%. As a result, an average of both signals was taken to be the reference signal.

The DO_2 radical in the Cl-initiated experiments was monitored by direct laser probing of the 000−000 band of the $\tilde{A}^2A' \leftarrow X^2A''$ electronic transition near 7023 cm^{-1}.[50] The tunable CW infrared radiation is generated by difference frequency mixing in temperature-tuned $LiNbO_3$.[51,52] The outputs of a single frequency, CW, diode-pumped laser operating at 1.06 μm and a tunable signal laser radiation coming from a ring dye laser operating around 609 nm are combined and rendered collinear into a $LiNbO_3$ crystal inside a temperature-controlled oven. The oven is heated to the necessary temperature to provide correct phase-matching for maximum IR generation. The ring dye laser is pumped by an 8 W, diode-pumped, frequency-doubled Nd:YVO_4 laser providing single frequency green output at 532 nm. Typical output powers are 500 and 600 mW for the single frequency 1.06 μm laser and tunable dye laser, respectively. Approximately 6 μW of tunable IR power at 1.4 μm is obtained with proper focusing of the input beams. A band-pass filter blocks the residual input laser beams while passing the IR beam. A traveling interferometer is used to monitor the output frequency of the ring dye laser.

Two techniques are employed to improve the detection sensitivity of the DO_2 probing: two-tone frequency modulation (FM) spectroscopy and a modified Herriott-type multipass flow cell.[53] Two-tone frequency modulation spectroscopy significantly reduces laser amplitude noise (by moving the detection bandpass to higher frequencies)[54,55] and thermal lensing noise (by the differential nature of FM signals).[56] Higher detection sensitivity is especially useful in the higher temperature experiments because of increases in the vibrational and rotational partition functions and the concomitant quantum state dilution which leads to smaller signals.

The use of a modified Herriott-type multipass flow cell[53] greatly increases the absorption path length, and hence the detection signal-to-noise ratio. The tunable IR power is passed multiple times (17 or 21 passes) through the flow cell. The flow cell is about 1.3 m long with CaF_2 windows and is surrounded by a commercial ceramic-fiber heater capable of reaching temperatures in excess of 1200 K. The gold-coated spherical mirrors that comprise the Herriott cell are located outside the flow cell and are separated by a distance of approximately 1.5 m. The photolysis beam, a 5-ns pulse from a Nd:YAG laser at 355 nm, which is telescoped and apertured to a diameter of 15 mm, passes through the center of the Herriott mirror. It travels on axis through the quartz flow cell and then passes through the center of the back Herriott mirror. The IR probe beam enters off axis through a notch in the back Herriott mirror, and traverses a circular pattern around the Herriott multipass mirrors, while mapping out a smaller circle in the center of the cell. Finally, the probe exits from a notch in the front Herriott mirror. After exiting, the probe beam goes through a band-pass filter and is focused onto a 125 MHz, low noise detector. This arrangement allows the infrared probe to overlap the UV photolysis beam only in the center of the flow cell, where the temperature is more readily controlled. The effective path length (i.e., overlapping path of photolysis and probe beams) is between 9 and 11 m, depending on the number of passes through the flow cell.

Gas flows are controlled by calibrated mass flow meters, and the total pressure is maintained by a butterfly valve at the exit of the cell, which operates under feedback from a capacitance manometer. The quartz flow cell is heated by three resistive elements, each under microprocessor control from a separate K-type thermocouple.

In the ethyl + O_2 experiments, typical gas concentrations were $[O_2] = 1.9 \times 10^{17}$ cm^{-3} (experiments were carried out in the range $[O_2] = 5.8 \times 10^{16}$ to 3.4×10^{17} cm^{-3}), $[Cl_2] = 2.8 \times 10^{15}$ cm^{-3} (range = 8.4×10^{14} to 5.6×10^{15} cm^{-3}), and $[C_2D_6] = 2.3 \times 10^{15}$ cm^{-3} (range = 7.6×10^{14} to 3.0×10^{15} cm^{-3}). Approximately 1−2% of the Cl_2 molecules were photolyzed in the beam path volume. In the propyl + O_2 experiments, typical gas concentrations are $[O_2] = 1.5 \times 10^{17}$ or 2.4×10^{17} cm^{-3} (range = 7.1×10^{16} to 3.0×10^{17} cm^{-3}), $[Cl_2] = 1.3 \times 10^{15}$ or 2.1×10^{15} cm^{-3} (range = 4.1×10^{14} to 4.3×10^{15} cm^{-3}), and $[C_3D_8] = 1.1 \times 10^{15}$ or 1.1×10^{16} cm^{-3} (range = 6.8×10^{14} to 1.8×10^{16} cm^{-3}). Higher photolysis powers were employed in these experiments, and approximately 3−7% of the Cl_2 molecules were photolyzed in the beam path volume region. The O_2 concentration is always kept at least 50 times greater than the Cl_2 concentration in order to minimize contributions from the alkyl + Cl_2 side reaction. In about 20% of the propyl experiments the concentration of C_3D_8 was a factor of 5−10 greater than the concentration of CD_3OD in the reference reactions. In all other experiments, including the ethyl experiments, the concentration of CD_3OD and the alkane are almost equal. As long as the concentration of alkane or methanol is high enough to intercept all Cl atoms, the absolute concentration is not critical. Helium is added as a buffer gas up to the desired total pressure. The $C_2D_5 + O_2$ experiments were carried out at five different temperatures (623, 673, 698, 723, and 748 K) and at several pressures ranging from 10 to 80 Torr. On the other hand, $C_3D_7 + O_2$ experiments were carried out at four different temperatures (623, 648, 673, and 703 K) and at pressures ranging from 25 to 75 Torr. At each temperature, the total pressure was varied except in the $C_2D_5 + O_2$ experiments at 623 and 748 K.

Direct Photolysis Experiments. The experimental system employed in the direct photolysis experiments is almost identical to the system used in a previous study of *n*-C_3H_7 and *i*-C_3H_7

radials with O_2,[38] and thus, only a brief description is given here. Nondeuterated and deuterated ethyl, *n*-propyl and isopropyl radicals are generated by 266 nm photolysis of ethyl, *n*-propyl and isopropyl iodides respectively:

$$RI + h\nu\ (266\ nm) \rightarrow I(^2P_{1/2}, ^2P_{3/2}) + R \qquad (6)$$

The main advantage of generating alkyl radicals by reaction 6 is that the experiments are isomer specific, which is particularly important in the study of propyl radicals with O_2. The HO_2 radical is monitored by laser probing in the 000−000 band of the $\tilde{A}^2A' \leftarrow X^2A''$ electronic transition near 7024 cm^{-1},[57] and in the overtone of the O−H stretch near 6626 cm^{-1}.[58−60] The DO_2 radical is again monitored using the 000−000 band of the $\tilde{A}^2A' \leftarrow X^2A''$ electronic transition near 7023 cm^{-1}.[50] The concentration of I atoms is deduced from a simultaneous measurement of the absorption on the spin−orbit transition of the I-atom photolysis coproduct, permitting transient HO_2 (and DO_2) FM signals to be scaled to the initial I-atom absorption. Under the assumption that every iodine atom is produced in conjunction with every alkyl radical, the initial I-atom concentration equals the initial alkyl radical concentration. However, because the HO_2 (and DO_2) line strength is not known, the yield of the HO_2 (and DO_2) radical cannot be directly derived from the present data, as it was in previous Cl-initiated alkyl + O_2 reactions. Nonetheless, the time profile of the I-atom concentration provides an additional experimental profile to demand consistency with the theoretical simulations.

External-cavity tunable diode lasers were employed to probe the time-resolved absorption profiles of HO_2 and DO_2. As in the Cl-initiated oxidation experiments, two-tone frequency modulation spectroscopy and a modified Herriott-type multipass flow cell are employed to increase the detection sensitivity. In order to further improve the signal-to-noise ratio, the diode laser probe beam is split into signal and reference beams. The reference beam impinges on a low noise detector (I_0) after traveling an equal path length as the signal beam through an analogous modified Herriott-type multipass arrangement open to atmospheric pressure. The signal beam is directed through the multipass flow cell and onto a second low noise detector (I). The time-resolved FM signal is monitored as the demodulated difference between balanced signal (I) and reference (I_0), permitting subtraction of common noise. Approximately 50 μW of IR power is incident on each detector. A commercial traveling-interferometer wavemeter is used to monitor the frequency of the diode laser beam.

The iodine atom concentration is probed by a second external-cavity diode laser tuned to the $^2P_{1/2} \leftarrow {}^2P_{3/2}$ transition at ∼1315 nm (i.e., $(F' = 3) \leftarrow (F'' = 4)$ hyperfine component of the ($^2P_{1/2} \leftarrow {}^2P_{3/2}$) spin orbit transition), after making a single-pass through the modified Herriott-type multipass flow cell. The transient I-atom absorption is monitored by subtracting the output of balanced signal (I) and reference (I_0) detectors. In order to stabilize the frequency output of the diode laser, a fraction of the laser beam is phase modulated, directed through a high-temperature cell (∼1100 K), in which I_2 is thermally dissociated to generate I atoms, and imaged on a fast IR detector. The resulting single-tone FM signal (after subsequent demodulation) is used as the "error signal" for a PID controller to automatically correct any frequency deviations away from line center.

Typical gas concentrations in the deuterated alkyl + O_2 study were $[O_2] = 1.5 \times 10^{17}$ cm^{-3} and [alkyl iodide] = 3×10^{15} cm^{-3}. Approximately 1−3% of the alkyl iodide molecules were photolyzed in the beam path volume. Helium is added to a total density of 3.65×10^{17} cm^{-3}. Experiments were carried out at three different temperatures (648, 673, and 703 K). At the relatively high levels of O_2 in these experiments, spin−orbit excited I ($^2P_{1/2}$) atoms (I^*) are quenched to the ground state very rapidly (on the order of less than a microsecond),[61−64] and thus, iodine atom concentrations can be easily derived from the probe laser path length (defined as the interaction path length between the photolysis laser and the 1315 nm probe) and the absolute absorption cross section of I atoms for the $F^* = 3 \leftarrow F = 4$ hyperfine transition at 1315.246 nm.[65,66] Experiments at lower O_2 concentrations were also carried out in the study of the nondeuterated isopropyl + O_2 reaction at a temperature of 703 K and a total density of 3.65×10^{17} cm^{-3}. In this set of experiments, the typical isopropyl iodide concentration was 1.5×10^{15} cm^{-3} and the O_2 concentration was varied from 1.9×10^{15} cm^{-3} to 1.1×10^{16} cm^{-3}. At these O_2 concentrations, spin−orbit excited I ($^2P_{1/2}$) atoms (I^*) are still quenched to the ground state fairly rapidly (a few tens of microseconds for the lowest O_2 experiments).[61−64]

Theory. The master equation simulations have been performed as described in previous work on ethyl + O_2 and propyl + O_2, using the stationary point energies calculated in previous works.[19,22,23,37,38] For ethyl + O_2 and *n*-propyl + O_2, the barrier heights, and indeed the full model, are precisely as described in an earlier work,[38] and thus, no further details are presented here. Minor adjustments to the isopropyl potential energy surface are performed with respect to a previous publication[38] and only these changes are discussed here. First, it is important to point out that in a previous publication[38] the $(CH_3)_2CHOO$ well depth employed in the simulations was inadvertently misstated. The $(CH_3)_2CHOO$ well depth was decreased from the *ab initio* value by 0.6 kcal mol^{-1} and, thus, was set at 36.2 kcal mol^{-1} below the energy of the reactants (not increased from the *ab initio* value by 1.3 kcal mol^{-1}, as was previously stated). In the current work, both the $(CH_3)_2CHOO$ well depth and the transition state for HO_2 elimination are further adjusted from their respective *ab initio* values. The $(CH_3)_2CHOO$ well depth is decreased from the *ab initio* value by 2.0 kcal mol^{-1}, and is now set at 34.8 kcal mol^{-1} below the energy of the reactants, and the transition state for HO_2 elimination is raised by 1 kcal mol^{-1} from the *ab initio* value of −7 kcal mol^{-1}, to 6 kcal mol^{-1} below the energy of the reactants.

As in previous works,[19,22,23,37,38] the results of the time-dependent master equation analysis of ethyl + O_2 and propyl + O_2 reactions have been reduced to a set of elementary reactions and phenomenological rate coefficients which include pathways for HO_2 and OH formation in the nondeuterated reactions and DO_2 and OD formation in the deuterated reactions. Vibrational frequencies and moments of inertia for the deuterated species are calculated at the same level as in the previous calculations of the nondeuterated isotopomers.[19,37,38] Phenomenological rate coefficients are obtained from solutions to the master equations using the methodology described by Klippenstein and Miller.[67] Tables 1 and 2 show the set of elementary reactions and phenomenological rate coefficients that are used to model the reactions of $C_2D_5 + O_2$ and $C_3D_7 + O_2$ at selected temperatures and pressures (see Tables for specific conditions) using the stationary point energies described above. Table 3 shows analogous results to the ones shown in Tables 1 and 2 but for $i\text{-}C_3H_7 + O_2$ at a total density of 3.65×10^{17} cm^{-3} using the modified stationary-point energies described above.

Comprehensive Kinetic Model. The calculated phenomenological rate coefficients for ethyl + O_2, *n*-propyl + O_2, and isopropyl + O_2 derived from the time-dependent master equations allows a model of the reaction systems to be

TABLE 1: Rate Coefficients for Relevant Reactions in the $C_2D_5 + O_2$ System Generated from Solutions to the Master Equation at Selected Temperatures and Pressures[a]

	$C_2D_5 + O_2 \rightarrow C_2D_5O_2$	$C_2D_5 + O_2 \rightarrow C_2D_4 + DO_2$	$C_2D_5O_2 \rightarrow C_2D_4 + DO_2$	$K_{eq}(C_2D_5 + O_2 \leftrightarrow C_2D_5O_2)$
623 K, 55 Torr	1.24×10^{-12}	6.91×10^{-14}	3.28	6.72×10^{-15}
650 K, 57.2 Torr	1.01×10^{-12}	6.91×10^{-14}	7.88	2.12×10^{-15}
673 K, 60 Torr	8.42×10^{-13}	6.94×10^{-14}	15.4	8.64×10^{-16}
25 Torr	4.71×10^{-13}	7.25×10^{-14}	9.09	
10 Torr	2.40×10^{-13}	7.55×10^{-14}	8.40	
700 K, 61.6 Torr	6.68×10^{-13}	6.94×10^{-14}	31.2	3.25×10^{-16}
750 K, 66 Torr	4.37×10^{-13}	6.95×10^{-14}	95.9	6.45×10^{-17}

[a] Units of cm^3 molecule^{-1} s^{-1} for second-order rate coefficients, s^{-1} for first-order rate coefficients, and cm^3 for equilibrium constants.

TABLE 2: Rate Coefficients for the *n*-$C_3D_7 + O_2$ and *i*-$C_3D_7 + O_2$ Systems Generated from Solutions to the Master Equation at Selected Temperatures and Pressures

reaction	k_{623}[a,b]	k_{648}[a,c]	k_{673}[a,c]	k_{703}[a,c]
n-$C_3D_7 + O_2 \rightarrow$ *n*-$C_3D_7O_2$	2.14×10^{-12}	1.52×10^{-12}	1.26×10^{-12}	9.90×10^{-13}
n-$C_3D_7 + O_2 \rightarrow CD_3CDCD_2OOD$	5.14×10^{-18}	3.32×10^{-18}	3.18×10^{-18}	3.19×10^{-18}
n-$C_3D_7 + O_2 \rightarrow C_3D_6 + DO_2$	3.90×10^{-14}	5.16×10^{-14}	5.55×10^{-14}	5.94×10^{-14}
n-$C_3D_7 + O_2 \rightarrow$ methyloxirane-d_6 + OD	4.51×10^{-15}	5.97×10^{-15}	6.41×10^{-15}	6.85×10^{-15}
n-$C_3D_7 + O_2 \rightarrow$ oxetane-d_6 + OD	1.26×10^{-16}	1.73×10^{-16}	2.20×10^{-16}	2.86×10^{-16}
n-$C_3D_7 + O_2 \rightarrow$ propanal-d_6 + OD	1.01×10^{-15}	1.38×10^{-15}	1.64×10^{-15}	1.98×10^{-15}
n-$C_3D_7O_2 \rightarrow$ *n*-$C_3D_7 + O_2$	391	810	1.80×10^{3}	4.21×10^{3}
n-$C_3D_7O_2 \rightarrow CD_3CDCD_2OOD$	9.16×10^{-2}	0.132	0.284	0.712
n-$C_3D_7O_2 \rightarrow C_3D_6 + DO_2$	13.2	27.6	59.5	135
n-$C_3D_7O_2 \rightarrow$ methyloxirane-d_6 + OD	1.53	3.24	6.94	15.6
n-$C_3D_7O_2 \rightarrow$ oxetane-d_6 + OD	4.30×10^{-3}	7.51×10^{-3}	1.82×10^{-2}	4.63×10^{-2}
n-$C_3D_7O_2 \rightarrow$ propanal-d_6 + OD	8.37×10^{-2}	0.157	0.372	0.925
$CD_3CDCD_2OOD \rightarrow$ *n*-$C_3D_7 + O_2$	1.52	2.16	4.19	9.38
$CD_3CDCD_2OOD \rightarrow$ *n*-$C_3D_7O_2$	92.2	74.6	94.0	119
$CD_3CDCD_2OOD \rightarrow C_3D_6 + DO_2$	1.81×10^{4}	1.27×10^{4}	1.67×10^{4}	2.24×10^{4}
$CD_3CDCD_2OOD \rightarrow$ methyloxirane-d_6 + OD	2.80×10^{6}	2.50×10^{6}	3.15×10^{6}	4.05×10^{6}
$CD_3CDCD_2OOD \rightarrow$ oxetane-d_6 + OD	1.76×10^{-5}	2.10×10^{-5}	4.46×10^{-5}	1.10×10^{-4}
$CD_3CDCD_2OOD \rightarrow$ propanal-d_6 + OD	3.35×10^{-4}	4.33×10^{-4}	8.99×10^{-4}	2.16×10^{-3}
i-$C_3D_7 + O_2 \rightarrow$ *i*-$C_3D_7O_2$	6.86×10^{-12}	4.22×10^{-12}	3.31×10^{-12}	2.44×10^{-12}
i-$C_3D_7 + O_2 \rightarrow$ *i*-C_3D_6OOD	1.04×10^{-16}	6.00×10^{-17}	5.11×10^{-17}	4.28×10^{-17}
i-$C_3D_7 + O_2 \rightarrow C_3D_6 + DO_2$	4.68×10^{-13}	5.35×10^{-13}	5.32×10^{-13}	5.24×10^{-13}
i-$C_3D_7 + O_2 \rightarrow$ methyloxirane-d_6 + OD	4.78×10^{-15}	5.52×10^{-15}	5.68×10^{-15}	5.82×10^{-15}
i-$C_3D_7 + O_2 \rightarrow C_2D_6CO$ + OD	2.94×10^{-16}	3.60×10^{-16}	4.24×10^{-16}	5.10×10^{-16}
i-$C_3D_7O_2 \rightarrow$ *i*-$C_3D_7 + O_2$	773	1.43×10^{3}	3.05×10^{3}	6.83×10^{3}
i-$C_3D_7O_2 \rightarrow$ *i*-C_3D_6OOD	0.120	0.208	0.477	1.25
i-$C_3D_7O_2 \rightarrow C_3D_6 + DO_2$	57.7	108	219	466
i-$C_3D_7O_2 \rightarrow$ methyloxirane-d_6 + OD	0.235	0.417	0.826	1.60
i-$C_3D_7O_2 \rightarrow C_2D_6CO$ + OD	1.60×10^{-3}			
i-$C_3D_6OOD \rightarrow$ *i*-$C_3D_7 + O_2$	317	367	574	960
i-$C_3D_6OOD \rightarrow$ *i*-$C_3D_7O_2$	2.18×10^{3}	1.90×10^{3}	2.32×10^{3}	2.80×10^{3}
i-$C_3D_6OOD \rightarrow C_3D_6 + DO_2$	2.92×10^{5}	2.42×10^{5}	3.16×10^{5}	4.23×10^{5}
i-$C_3D_6OOD \rightarrow$ methyloxirane-d_6 + OD	1.96×10^{6}	1.85×10^{6}	2.35×10^{6}	3.05×10^{6}
i-$C_3D_6OOD \rightarrow C_2D_6CO$ + OD	1.24×10^{-3}	8.39×10^{-4}	1.25×10^{-3}	1.94×10^{-3}

[a] Units of cm^3 molecule^{-1} s^{-1} for second-order reactions and s^{-1} for first-order reactions. [b] Total pressure of 45 Torr. [c] Total pressure of 25 Torr.

constructed by using the elementary reactions involved in the three reaction systems. The experimentally observed HO_2 and DO_2 time traces can then be compared to predictions of this model. For these calculated phenomenological rate coefficients to reproduce the observed experimental data, rate coefficients must be added to the model that describe the loss and formation of all other radicals involved in the experiment, as performed previously.[19,38] Literature rate coefficients associated with these reactions are combined with the rate coefficients derived from solutions to master equations to form integrated rate equation models that describe HO_2 and DO_2 formation and removal mechanisms important in the time domain of the experiment. The reactions and rate coefficients used in the deuterated models are listed in Table 4 for $C_2D_5 + O_2$ and in Table 5 for $C_3D_7 + O_2$. Chlorine and iodine reactions are included jointly in the two master kinetic models. The experiments are initiated by either photolysis of Cl_2 or photolysis of alkyl iodides, and the model is adapted by setting the initial Cl or I-atom concentration accordingly.

In previous publications,[19,38] it was possible to use available literature rate coefficients for many reactions in the kinetics models and make estimates based on similar reactions when no literature values were reported (for example, estimating rate coefficients based on similar reactions in the more thoroughly studied CH_3/O_2 system or estimating rate coefficients that have not been determined experimentally for the C_3H_7/O_2 systems based on analogous rate constants in the C_2H_5/O_2 system). A similar methodology is employed in the current work. Nonetheless, in the deuterated systems only very few literature values are available, and many of these studies have only been carried out at room temperature. Therefore, rate coefficients that are not available in the literature are estimated based on the analogous nondeuterated reactions.

One important reaction that has not been experimentally studied at the temperatures of the present investigations is the self-reaction of DO_2 radicals. Only four experimental studies are available from the literature of which two studies have only been carried out at room temperature[68,69] and the other two over

TABLE 3: Rate Coefficients for the *i*-$C_3H_7 + O_2$ System Generated from Solutions to the Master Equation at a Total Density of 3.65×10^{17} cm^{-3}

reaction	k_{623}[a]	k_{648}[a]	k_{673}[a]	k_{703}[a]
$i\text{-}C_3H_7 + O_2 \rightarrow i\text{-}C_3H_7O_2$	2.37×10^{-12}	1.91×10^{-12}	1.52×10^{-12}	1.14×10^{-12}
$i\text{-}C_3H_7 + O_2 \rightarrow i\text{-}C_3H_6OOH$	7.11×10^{-16}	6.00×10^{-16}	5.08×10^{-16}	4.15×10^{-16}
$i\text{-}C_3H_7 + O_2 \rightarrow C_3H_6 + HO_2$	1.11×10^{-12}	1.07×10^{-12}	1.02×10^{-12}	9.72×10^{-13}
$i\text{-}C_3H_7 + O_2 \rightarrow$ methyloxirane + OH	1.95×10^{-14}	1.91×10^{-14}	1.87×10^{-14}	1.82×10^{-14}
$i\text{-}C_3H_7 + O_2 \rightarrow C_2H_6CO + OH$	8.13×10^{-16}	9.17×10^{-16}	1.03×10^{-15}	1.18×10^{-15}
$i\text{-}C_3H_7O_2 \rightarrow i\text{-}C_3H_7 + O_2$	566	1.31×10^{3}	2.78×10^{3}	6.12×10^{3}
$i\text{-}C_3H_7O_2 \rightarrow i\text{-}C_3H_6OOH$	1.63	3.56	7.42	17.0
$i\text{-}C_3H_7O_2 \rightarrow C_3H_6 + HO_2$	204	433	849	1.73×10^{3}
$i\text{-}C_3H_7O_2 \rightarrow$ methyloxirane + OH	1.43	2.91	5.29	9.15
$i\text{-}C_3H_7O_2 \rightarrow C_2H_6CO + OH$	6.72×10^{-3}	1.42×10^{-2}	2.75×10^{-2}	5.29×10^{-2}
$i\text{-}C_3H_6OOH \rightarrow i\text{-}C_3H_7 + O_2$	1.78×10^{3}	2.78×10^{3}	4.22×10^{3}	6.67×10^{3}
$i\text{-}C_3H_6OOH \rightarrow i\text{-}C_3H_7O_2$	1.23×10^{4}	1.52×10^{4}	1.83×10^{4}	2.20×10^{4}
$i\text{-}C_3H_6OOH \rightarrow C_3H_6 + HO_2$	5.53×10^{4}	7.89×10^{4}	1.09×10^{5}	1.53×10^{5}
$i\text{-}C_3H_6OOH \rightarrow$ methyloxirane + OH	9.93×10^{5}	1.33×10^{6}	1.74×10^{6}	2.31×10^{6}
$i\text{-}C_3H_6OOH \rightarrow C_2H_6CO + OH$	2.86×10^{-2}	4.45×10^{-2}	6.71×10^{-2}	0.105

[a] Units of cm^3 molecule^{-1} s^{-1} for second-order reactions and s^{-1} for first-order reactions.

the temperature range of 230−420 K.[70,71] Because the rate coefficient for the self-reaction of DO_2 is an important input to the kinetics models, experiments are carried out to estimate the kinetic isotope effect for this reaction at 703 K. The reference system of Cl-initiated methanol oxidation (i.e., reactions 1, 4, 5) is an excellent method to study the kinetics of the DO_2 self-reaction because the removal of DO_2 is largely dominated by that reaction. Back to back experiments are carried out, first with normal isotopic abundance methanol, CH_3OH, and then with fully deuterated methanol, CD_3OD. Under these conditions the DO_2 and HO_2 signal (depending on which system is being run) rises rapidly and then decays according to their self-reaction rate coefficients. The peroxyl radical concentration is assumed to be identical in the two experiments, so the ratio of the HO_2 to DO_2 self-reaction rate coefficients is obtained from a second-order rate analysis. Particular care is taken to maintain all other photolysis conditions identical (i.e., concentrations of He, O_2 and Cl_2 and photolysis laser powers). The spatial uniformity of the radical concentration will affect measurements of second-order decays, albeit modestly;[72] the present experiments use an apertured photolysis beam (to reduce radial differences in illumination) and are carried out in an optically thin medium (photolysis absorptions less than 10%). These experiments result in a kinetic isotope effect of approximately 1.25 at 703 K. The measured kinetic isotope effect of 1.25 is then assumed to remain constant over the entire range of temperatures studied in this work (i.e., 623−748 K).

Results and Discussion

Because the reaction of ethyl + O_2 is the simplest system where HO_2 and alkene formation are possible, it is a good place to start looking at the kinetic isotope effect. Figure 1 shows the formation of DO_2 from Cl-initiated oxidation of C_2D_6 compared to the HO_2 formation from C_2H_6 at a temperature of 698 K and a total pressure of 61.5 Torr. Figure 1 concentrates on the first 12 milliseconds after the UV photolysis flash where the HO_2 and DO_2 production depend primarily on the ethyl + O_2 reaction and the effects of the additional chemistry are still small. Similarly to the nondeuterated ethyl + O_2 reaction[6,19,38] and to other nondeuterated alkyl + O_2 reactions,[19,33−38] the production of DO_2 displays two clearly separated components: a prompt DO_2, which is observed immediately following the UV flash and which cannot be temporally resolved under the current experimental conditions, and a second, slower delayed rise. Two observations are evident from Figure 1: the prompt DO_2 yield (resulting from the $C_2D_5 + O_2$ reaction) is somewhat (∼50%) smaller than the HO_2 yield (resulting from the $C_2H_5 + O_2$ reaction) and the secondary production (or "delayed" production) is more than 2 times faster for HO_2 than for DO_2. It is instructive to review the interpretation of both prompt and delayed HO_2 in order to understand these observations. The prompt yield is the fraction of HO_2, or DO_2, at the establishment of the steady-state between addition and redissociation and it is governed by the competition between collisional stabilization and direct reaction (i.e., concerted elimination of HO_2, or DO_2, from the chemically activated RO_2^*). The delayed time constant arises from the dissociation of the thermalized RO_2 species, which can be accomplished either by dissociation of RO_2 to R + O_2 followed by direct reaction or by thermal elimination of HO_2, or DO_2, from the stabilized RO_2 radical via the concerted elimination transition state. The deuterated RO_2 adduct has a higher density of states than its nondeuterated counterpart, resulting in more efficient stabilization of the deuterated species. More efficient stabilization leads to a slower direct reaction rate, which lowers the prompt yield. Furthermore, the change in zero-point energies yields a higher (by approximately 0.9 kcal mol^{-1}) effective barrier for DO_2 elimination than for HO_2 elimination. This results in a slower escape of radicals from the R + O_2 ↔ RO_2 quasi-equilibrium, which leads to slower delayed DO_2 formation relative to the nondeuterated species.

Naturally, the next goal is to simulate the DO_2 profiles with the integrated rate equation models. Figure 2 shows a comparison of the predicted and observed DO_2 signals at several temperatures and a total density of 8.45×10^{17} cm^{-3} in the Cl-initiated $C_2D_5 + O_2$ experiments. The agreement between the experimental data and the model is good at all the experimental conditions investigated, especially on the early time after the photolysis where the DO_2 production depends predominantly on the $C_2D_5 + O_2$ reaction. A similar level of agreement between the experiment and the kinetic model is found while varying the concentrations of O_2, Cl, and C_2D_6 by factors ranging from 4 to 6. The largest disagreements are found for the prompt yields of DO_2 at the lowest temperatures investigated, where the model is ∼60% of that observed in the experiment. The rise time of the DO_2 signal is underpredicted by at most 35%. The fit of the decay becomes poorer at higher temperature, possibly because of inaccuracy in the rate coefficient for the DO_2 self-reaction or because of an increasing role of radial diffusion. At the densities of the present experiments, radial diffusion is approximately equivalent to a first-order loss of 10 s^{-1} at room temperature (axial diffusion has a negligible effect on the signal). Because the reactions of interest

TABLE 4: Reactions and Rate Coefficients Used To Model the DO_2 and I Signals from the Cl-Initiated Oxidation of Ethane and the Photodissociation of C_2D_5I[a]

reaction	A[b]	n	E_a/R (K)	ref[c]
$C_2D_5 + O_2 \rightarrow$ products				ME[d]
$C_2D_6 + Cl \rightarrow DCl + C_2D_5$	3.4×10^{-11}	0.7	−150	74
$DO_2 + DO_2 \rightarrow O_2 + D_2O_2$	1.76×10^{-13}		−600	75[e]
$C_2D_5O_2 + C_2D_5O_2 \rightarrow 2C_2D_5O + O_2$	$\phi \times 8.5 \times 10^{-14}$		125	76[f]
$C_2D_5O_2 + C_2D_5O_2 \rightarrow C_2D_5OD + CD_3CDO$	$(1 - \phi) \times 8.5 \times 10^{-14}$		125	76[f]
$C_2D_5O_2 + DO_2 \rightarrow C_2D_5O_2D + O_2$	6.9×10^{-13}		−702	77
$C_2D_5 + C_2D_5 \rightarrow$ products	1.99×10^{-11}			78
$C_2D_5 + C_2D_5O_2 \rightarrow 2C_2D_5O$	4.0×10^{-11}			79[g]
$C_2D_5 + DO_2 \rightarrow OD + C_2D_5O$	3.3×10^{-11}			79[g]
$C_2D_5 + DO_2 \rightarrow O_2 + C_2D_6$	6.0×10^{-12}			79[g]
$C_2D_5 + C_2D_5O \rightarrow (C_2D_5)_2O$	2.0×10^{-12}			80
$C_2D_5O + O_2 \rightarrow DO_2 + C_2D_4O$	2.4×10^{-14}		325	81
$C_2D_5O + DO_2 \rightarrow D_2O_2 + C_2D_4O$	5.0×10^{-13}			79[g]
$C_2D_5O + C_2D_5O_2 \rightarrow C_2D_5OOD + C_2D_4O$	5.0×10^{-13}			79[g]
$C_2D_5O + C_2D_5O \rightarrow C_2D_5OD + CD_3CDO$	6.0×10^{-11}			*h*
$C_2D_5O \rightarrow CD_3 + CD_2O$	7.9×10^{13}		11060	82
$C_2D_5O \rightarrow D + C_2D_4O$	6.3×10^{13}		12100	82
$C_2D_5O \rightarrow CD_3CDOD$	5.0×10^{13}		13580	82
$C_2D_5O \rightarrow CD_2CD_2OD$	7.9×10^{12}		14830	82
$CD_3 + O_2 + M \rightarrow CD_3O_2 + M$				*i*
$CD_3O_2 + CD_3O_2 \rightarrow 2CD_3O + O_2$	9.2×10^{-14}		−390	76
$CD_3O_2 + C_2D_5O_2 \rightarrow CD_3 + C_2D_5O + O_2$	1.4×10^{-13}			*j*
$CD_3O + O_2 \rightarrow CD_2O + DO_2$	7.2×10^{-14}		1080	83
$D + O_2 + M \rightarrow DO_2 + M$				*k*
$Cl + C_2D_5 \rightarrow DCl + C_2D_4$	7.57×10^{-10}		290	84
$Cl + C_2D_5O_2 \rightarrow ClO + C_2D_5O$	7.7×10^{-11}			85
$Cl + C_2D_5O_2 \rightarrow DCl + C_2D_4O$	7.3×10^{-11}			85
$Cl + DO_2 \rightarrow ClO + OD$	4.1×10^{-11}		450	75
$Cl + DO_2 \rightarrow DCl + O_2$	1.8×10^{-11}		−170	75
$Cl + C_2D_5O \rightarrow C_2D_4O + DCl$	1.9×10^{-11}			80[g]
$Cl_2 + C_2D_5 \rightarrow C_2D_5Cl + Cl$	1.3×10^{-11}		−120	86
$Cl_2 + CD_3 \rightarrow Cl + CD_3Cl$	4.8×10^{-12}		240	86
$Cl_2 + D \rightarrow Cl + DCl$	1.4×10^{-11}		209	*l*
$I + I + M \rightarrow I_2 + M$	5.5×10^{-34}		−575	87
$I + DO_2 \rightarrow DI + O_2$	1.47×10^{-11}		1090	88
$I + C_2D_5I \rightarrow I_2 + C_2D_5I$	3.85×10^{-10}		8600	*m*
$I + C_2D_5 \rightarrow DI + C_2D_4$	3.83×10^{-11}			*n*
$I + C_2D_5O_2 \rightarrow DOI + CD_3CDO$	2.0×10^{-12}			38
$I + X \rightarrow$ products	1.0×10^{-11}			38
$I_2 + OD \rightarrow DOI + I$	2.1×10^{-10}			81
$I_2 + C_2D_5 \rightarrow I + C_2D_5I$	5.0×10^{-11}			89
$DI + OD \rightarrow D_2O + I$	7.05×10^{-12}		−440	*o*
$DI + C_2D_5 \rightarrow I + C_2D_6$	2.54×10^{-12}		−384	*p*
$C_2D_5I \rightarrow C_2D_5 + I$	1.41×10^{13}		25201	*q*
$C_2D_5I \rightarrow DI + C_2D_4$	3.97×10^{13}		26602	*q*

[a] Rate coefficients are written in the form $A(T/298)^n e^{-Ea/RT}$ unless otherwise noted. [b] Units of s^{-1} for first-order reactions, cm^3 molecule^{-1} s^{-1} for second-order reactions and (cm^6 molecule^{-2} s^{-1}) for third-order reactions. [c] Rate coefficients are estimated based on the reactions of analogous nondeuterated species, unless otherwise noted. [d] Rate coefficients are generated from solutions to the master equation (ME).[23] [e] Rate coefficients are calculated based on the recommendation of Atkinson et al.[75] and the kinetic isotope effect obtained from this work (i.e., 1.25). [f] The branching fraction is fit to the function $\phi = 1.33 \exp(-209/T)$.[76] [g] Estimated on the basis of the CH_3/O_2 system.[79] [h] Calculated based on an average of three literature studies.[79,90,91] [i] Effective second-order rate coefficient is calculated from the expression given by DeMore et al.,[49] where $k_0^{300} = 1.2 \times 10^{-30}$ cm^6 molecule^{-2} s^{-1}, $k_\infty^{300} = 1.4 \times 10^{-12}$ cm^3 molecule^{-1} s^{-1}, $n = 3.0$, $m = 1.7$, and $F_{cent} = 0.46$. k_0^{300}, k_∞^{300}, and F_{cent} are taken from actual room temperature measurements of $CD_3 + O_2$.[92] The temperature dependence is estimated from the analogous $CH_3 + O_2$ reaction.[49] [j] Calculated based on an average of the rate coefficient of reaction $C_2D_5O_2 + C_2D_5O_2$ and the rate coefficient of reaction $CD_3O_2 + CD_3O_2$, assuming no temperature dependence (as estimated by Kaiser).[7] [k] Effective second-order rate coefficient is calculated from the expression given by DeMore et al.[49] where $k_0^{300} = 5.7 \times 10^{-32}$ cm^6 molecule^{-2} s^{-1}, $k_\infty^{300} = 7.5 \times 10^{-11}$ cm^3 molecule^{-1} s^{-1}, $n = 1.6$, $m = 0$, and $F_{cent} = 0.6$. [l] Pre-exponential factor, A, is taken from an absolute value measurement of the $D + Cl_2$ reaction,[93] and the temperature dependence is estimated from the analogous $H + Cl_2$ reaction.[94] [m] Rate coefficients are estimated based on the analogous $I + C_2H_5I$ reaction[95] multiplied by 2.3, which is calculated based on the negative kinetic isotope effect measured for the $I + CH_3I/I + CD_3I$ reaction system.[96] [n] Rate coefficients are estimated based on the analogous $I + C_2H_5$ reaction[97] multiplied by 3.3, which is calculated based on the negative kinetic isotope effect measured for the $I + CH_3/I + CD_3$ reaction system.[97] [o] Rate coefficients are estimated based on the analogous HI + OH reaction[81] divided by 2.3, which is calculated based on the kinetic isotope effect measured for the HCl + OH/ DCl + OD reaction system.[98] [p] Rate coefficients are estimated based on the analogous $HI + C_2H_5$ reaction[99] divided by 1.8, which is calculated based on the kinetic isotope effect measured for the HI + *tert*-C_4H_9/DI + *tert*-C_4H_9 reaction system.[100] [q] Rate coefficients are estimated based on the analogous decomposition of C_2H_5I[101] divided by 3.2, which is calculated based on the kinetic isotope effect measured for the CH_3I/CD_3I decomposition system.[102]

are exhibited in the early part of the signals, diffusion is neglected in the model.

Similar to the nondeuterated alkyl radical oxidation systems,[23,38] both the prompt and the delayed production of DO_2 increase as a function of temperature. The time scale for the delayed production of HO_2 exhibits an apparent activation energy of approximately 25 kcal mol^{-1} for a range of $R + O_2$ reactions,[37,39] and the deuterated reactions appear similar. However, the delayed production cannot be directly attributed to an elementary rate coefficient,[40] but is a convolution of

TABLE 5: Reactions and Rate Coefficients Used To Model the DO_2 and I Signals from the Cl-Initiated Oxidation of Propane and the Photodissociation of *n*-C_3D_7I and *i*-C_3D_7I[a]

reaction	A[b]	n	E_a/R (K)	ref[c]
i-$C_3D_7 + O_2 \rightarrow$ products				ME[d]
n-$C_3D_7 + O_2 \rightarrow$ products				ME[d]
$C_3D_8 + Cl \rightarrow DCl + n\text{-}C_3D_7$	2.8×10^{-11}		212	*e*
$C_3D_8 + Cl \rightarrow DCl + i\text{-}C_3D_7$	5.4×10^{-11}		86	*f*
$C_3D_8 + OD \rightarrow n\text{-}C_3D_7 + D_2O$	$\phi \times 4.3 \times 10^{-13}$	2.53	14.6	*g*
$C_3D_8 + OD \rightarrow i\text{-}C_3D_7 + D_2O$	$(1 - \phi) \times 4.3 \times 10^{-13}$	2.53	14.6	*g*
$DO_2 + DO_2 \rightarrow O_2 + D_2O_2$	1.76×10^{-13}		−600	75[h]
$OD + DO_2 \rightarrow D_2O + O_2$	4.8×10^{-11}		−250	75
$OD + OD \rightarrow O + D_2O$	2.5×10^{-13}		−170	103[i]
$OD + OD + M \rightarrow D_2O_2 + M$	6.89×10^{-31}	−0.80		75
$n\text{-}C_3D_7O_2 + n\text{-}C_3D_7O_2 \rightarrow 2n\text{-}C_3D_7O + O_2$	$\phi \times 3.0 \times 10^{-13}$			75[j]
$n\text{-}C_3D_7O_2 + n\text{-}C_3D_7O_2 \rightarrow n\text{-}C_3D_7OD + C_2D_5CDO + O_2$	$(1 - \phi) \times 3.0 \times 10^{-13}$			75[j]
$i\text{-}C_3D_7O_2 + i\text{-}C_3D_7O_2 \rightarrow 2i\text{-}C_3D_7O + O_2$	$\phi \times 1.6 \times 10^{-12}$		2200	75[j]
$i\text{-}C_3D_7O_2 + i\text{-}C_3D_7O_2 \rightarrow i\text{-}C_3D_7OD + CD_3COCD_3 + O_2$	$(1 - \phi) \times 1.6 \times 10^{-12}$		2200	75[j]
$n\text{-}C_3D_7O_2 + i\text{-}C_3D_7O_2 \rightarrow n\text{-}C_3D_7O + i\text{-}C_3D_7O + O_2$				*j*, *k*
$n\text{-}C_3D_7O_2 + i\text{-}C_3D_7O_2 \rightarrow$ products				*j*, *k*
$n\text{-}C_3D_7O_2 + DO_2 \rightarrow n\text{-}C_3D_7O_2D + O_2$	6.9×10^{-13}		−702	*l*
$i\text{-}C_3D_7O_2 + DO_2 \rightarrow i\text{-}C_3D_7O_2D + O_2$	6.9×10^{-13}		−702	*l*
$n\text{-}C_3D_7O_2 + OD \rightarrow DO_2 + n\text{-}C_3D_7O$	4.0×10^{-11}			*m*
$i\text{-}C_3D_7O_2 + OD \rightarrow DO_2 + i\text{-}C_3D_7O$	4.0×10^{-11}			*m*
$C_3D_6OOD + O_2 \rightarrow DOOC_3D_6O_2$	3.98×10^{-12}	−0.44		*n*
$DOOC_3D_6O_2 \rightarrow C_3D_6OOD + O_2$	7.11×10^{16}	−2.45	17665	*n*
$DOOC_3D_6O_2 \rightarrow OD + DOOC_3D_5O$	1.98×10^{10}	3.27	13954	*n*
$DOOC_3D_6O_2 \rightarrow OD + DOOC_3D_5O$	1.37×10^{11}	3.19	19588	*n*
$DOOC_3D_6O_2 \rightarrow OD + OOC_3D_6O$	3.0×10^{15}		21905	*n*
$DOOC_3D_6O_2 \rightarrow DO_2 + C_3D_6O_2$	4.17×10^{10}	3.51	14331	*n*
$n\text{-}C_3D_7 + OD \rightarrow C_3D_6 + D_2O$	4.0×10^{-11}			104
$i\text{-}C_3D_7 + OD \rightarrow C_3D_6 + D_2O$	4.0×10^{-11}			104
$n\text{-}C_3D_7 + n\text{-}C_3D_7 \rightarrow n\text{-}C_6D_{14}$	1.7×10^{-11}			104
$n\text{-}C_3D_7 + n\text{-}C_3D_7 \rightarrow C_3D_6 + C_3D_8$	2.8×10^{-12}			104
$i\text{-}C_3D_7 + i\text{-}C_3D_7 \rightarrow i\text{-}C_6D_{14}$	1.0×10^{-11}	−0.7		104
$i\text{-}C_3D_7 + i\text{-}C_3D_7 \rightarrow C_3D_6 + C_3D_8$	6.5×10^{-12}	−0.7		104
$i\text{-}C_3D_7 + n\text{-}C_3D_7 \rightarrow C_6D_{14}$	2.91×10^{-11}	−0.35		104
$i\text{-}C_3D_7 + n\text{-}C_3D_7 \rightarrow C_3D_6 + C_3D_8$	1.16×10^{-11}	−0.35		104
$i\text{-}C_3D_7 + i\text{-}C_3D_7O_2 \rightarrow 2i\text{-}C_3D_7O$	1.66×10^{-11}			105
$i\text{-}C_3D_7 + n\text{-}C_3D_7O_2 \rightarrow i\text{-}C_3D_7O + n\text{-}C_3D_7O$	1.66×10^{-11}			*o*
$n\text{-}C_3D_7 + n\text{-}C_3D_7O_2 \rightarrow 2n\text{-}C_3D_7O$	1.66×10^{-11}			*o*
$n\text{-}C_3D_7 + i\text{-}C_3D_7O_2 \rightarrow i\text{-}C_3D_7O + n\text{-}C_3D_7O$	1.66×10^{-11}			*o*
$n\text{-}C_3D_7 + DO_2 \rightarrow OD + n\text{-}C_3D_7O$	3.3×10^{-11}			*p*
$i\text{-}C_3D_7 + DO_2 \rightarrow OD + i\text{-}C_3D_7O$	3.3×10^{-11}			*p*
$n\text{-}C_3D_7 + DO_2 \rightarrow O_2 + C_3D_8$	6.0×10^{-12}			*p*
$i\text{-}C_3D_7 + DO_2 \rightarrow O_2 + C_3D_8$	6.0×10^{-12}			*p*
$n\text{-}C_3D_7 + n\text{-}C_3D_7O \rightarrow n\text{-}(C_3D_7)_2O$	2.0×10^{-12}			*q*
$i\text{-}C_3D_7 + i\text{-}C_3D_7O \rightarrow i\text{-}(C_3D_7)_2O$	2.0×10^{-12}			*q*
$n\text{-}C_3D_7 + i\text{-}C_3D_7O \rightarrow (C_3D_7)_2O$	2.0×10^{-12}			*q*
$i\text{-}C_3D_7 + n\text{-}C_3D_7O \rightarrow (C_3D_7)_2O$	2.0×10^{-12}			*q*
$n\text{-}C_3D_7O + OD \rightarrow C_3D_6O + D_2O$	3.0×10^{-11}			*p*
$i\text{-}C_3D_7O + OD \rightarrow C_3D_6O + D_2O$	3.0×10^{-11}			*p*
$i\text{-}C_3D_7O + O_2 \rightarrow DO_2 + C_3D_6O$	1.6×10^{-14}		264.6	106
$n\text{-}C_3D_7O + O_2 \rightarrow DO_2 + C_3D_6O$	2.5×10^{-14}		240.6	106
$n\text{-}C_3D_7O + DO_2 \rightarrow D_2O_2 + C_3D_6O$	5.0×10^{-13}			*p*
$i\text{-}C_3D_7O + DO_2 \rightarrow D_2O_2 + C_3D_6O$	5.0×10^{-13}			*p*
$n\text{-}C_3D_7O + n\text{-}C_3D_7O_2 \rightarrow n\text{-}C_3D_7OOD + C_3D_6O$	5.0×10^{-13}			*p*
$i\text{-}C_3D_7O + i\text{-}C_3D_7O_2 \rightarrow i\text{-}C_3D_7OOD + C_3D_6O$	5.0×10^{-13}			*p*
$n\text{-}C_3D_7O + i\text{-}C_3D_7O_2 \rightarrow i\text{-}C_3D_7OOD + C_3D_6O$	5.0×10^{-13}			*p*
$i\text{-}C_3D_7O + n\text{-}C_3D_7O_2 \rightarrow n\text{-}C_3D_7OOD + C_3D_6O$	5.0×10^{-13}			*p*
$n\text{-}C_3D_7O + n\text{-}C_3D_7O \rightarrow n\text{-}C_3D_7OD + C_3D_6O$	6.0×10^{-11}			*r*
$i\text{-}C_3D_7O + i\text{-}C_3D_7O \rightarrow i\text{-}C_3D_7OD + C_3D_6O$	6.0×10^{-11}			*r*
$n\text{-}C_3D_7O + i\text{-}C_3D_7O \rightarrow C_3D_7OD + C_3D_6O$	6.0×10^{-11}			*r*
$i\text{-}C_3D_7O \rightarrow D + CO(CD_3)_2$	2.0×10^{14}		10800	107
$i\text{-}C_3D_7O \rightarrow CD_3 + CD_3CDO$	3.98×10^{14}		8660	107
$n\text{-}C_3D_7O \rightarrow C_2D_5 + CD_2O$	5.01×10^{13}		7850	108
$CD_3 + O_2 + M \rightarrow CD_3O_2 + M$				*s*
$CD_3O_2 + CD_3O_2 \rightarrow 2CD_3O + O_2$	9.2×10^{-14}		−390	76
$CD_3O + O_2 \rightarrow CD_2O + DO_2$	7.2×10^{-14}		1080	83
$C_2D_5 + C_2D_5 \rightarrow$ products	1.99×10^{-11}			78
$C_2D_5 + DO_2 \rightarrow OD + C_2D_5O$	3.3×10^{-11}			79p
$C_2D_5 + DO_2 \rightarrow O_2 + C_2D_6$	6.0×10^{-12}			79p
$C_2D_5 + C_2D_5O \rightarrow (C_2D_5)_2O$	2.0×10^{-12}			80
$D + O_2 + M \rightarrow DO_2 + M$				*t*
$n\text{-}C_3D_7 \rightarrow C_3D_6 + D$	3.98×10^{13}		17608	109
$n\text{-}C_3D_7 \rightarrow C_2D_4 + CD_3$	6.95×10^{12}	−0.1	15211	110
$i\text{-}C_3D_7 \rightarrow C_3D_6 + D$	2.19×10^{12}	1.83	17819	111

TABLE 5: Continued

reaction	A^b	n	E_a/R (K)	ref[c]
i-$C_3D_7 \rightarrow C_2D_4 + CD_3$	3.98×10^{10}		14816	112
$Cl + n$-$C_3D_7 \rightarrow DCl + C_3D_6$	7.57×10^{-10}		290	*u*
$Cl + i$-$C_3D_7 \rightarrow DCl + C_3D_6$	7.57×10^{-10}		290	*u*
$Cl + n$-$C_3D_7O_2 \rightarrow ClO + n$-$C_3D_7O$	7.7×10^{-11}			*v*
$Cl + n$-$C_3D_7O_2 \rightarrow DCl + C_3D_6O_2$	7.3×10^{-11}			*v*
$Cl + i$-$C_3D_7O_2 \rightarrow ClO + i$-$C_3D_7O$	7.7×10^{-11}			*v*
$Cl + i$-$C_3D_7O_2 \rightarrow DCl + C_3D_6O_2$	7.3×10^{-11}			*v*
$Cl + DO_2 \rightarrow ClO + OD$	4.1×10^{-11}		450	75
$Cl + DO_2 \rightarrow DCl + O_2$	1.8×10^{-11}		−170	75
$Cl + n$-$C_3D_7O \rightarrow C_3D_6O + DCl$	1.9×10^{-11}			113[p]
$Cl + i$-$C_3D_7O \rightarrow C_3D_6O + DCl$	1.9×10^{-11}			113[p]
$Cl_2 + i$-$C_3D_7 \rightarrow Cl + i$-$C_3D_7Cl$	2.51×10^{-11}		−240	86
$Cl_2 + n$-$C_3D_7 \rightarrow Cl + n$-$C_3D_7Cl$	2.51×10^{-11}		−240	*w*
$Cl_2 + CD_3 \rightarrow Cl + CD_3Cl$	4.8×10^{-12}		240	86
$Cl_2 + D \rightarrow Cl + DCl$	1.4×10^{-11}		209	*x*
$I + I + M \rightarrow I_2 + M$	5.5×10^{-34}		−575	87
$I + DO_2 \rightarrow DI + O_2$	1.47×10^{-11}		1090	88
$I + n$-$C_3D_7I \rightarrow I_2 + n$-$C_3D_7$	4.77×10^{-10}		9301	*y*
$I + i$-$C_3D_7I \rightarrow I_2 + i$-$C_3D_7$	4.77×10^{-10}		9301	*z*
$I + n$-$C_3D_7 \rightarrow DI + C_3D_6$	3.83×10^{-11}			*aa*
$I + i$-$C_3D_7 \rightarrow DI + C_3D_6$	3.83×10^{-11}			*aa*
$I + n$-$C_3D_7O_2 \rightarrow DOI + C_2D_5CDO$	2.0×10^{-12}			38
$I + i$-$C_3D_7O_2 \rightarrow DOI + CD_3COCD_3$	2.0×10^{-12}			38
$I + X \rightarrow$ products	1.0×10^{-11}			38
$I_2 + OD \rightarrow DOI + I$	2.1×10^{-10}			81
$I_2 + n$-$C_3D_7 \rightarrow n$-$C_3D_7I + I$	5.0×10^{-11}			89
$I_2 + i$-$C_3D_7 \rightarrow i$-$C_3D_7I + I$	5.0×10^{-11}			*ab*
$DI + OD \rightarrow D_2O + I$	7.05×10^{-12}		−440	*ac*
$DI + n$-$C_3D_7 \rightarrow I + C_3D_8$	2.22×10^{-12}		−613	*ad*
$DI + i$-$C_3D_7 \rightarrow I + C_3D_8$	2.22×10^{-12}		−613	*ae*
n-$C_3D_7I \rightarrow n$-$C_3D_7 + I$	3.13×10^{12}		25201	*af*
n-$C_3D_7I \rightarrow DI + C_3D_6$	3.13×10^{12}		25201	*af*
i-$C_3D_7I \rightarrow DI + C_3D_6$	1.46×10^{13}		22701	*ag*

[a] Rate coefficients are written in the form $A(T/298)^n e^{-Ea/RT}$ unless otherwise noted. [b] Units of s^{-1} for first-order reactions, cm^3 $molecule^{-1}$ s^{-1} for second-order reactions and (cm^6 $molecule^{-2}$ s^{-1}) for third-order reactions. [c] Rate coefficients are estimated based on the reactions of analogous nondeuterated species, unless otherwise noted. [d] Rate coefficients generated from solutions to the Master Equation (ME) (see Tables 2 and 3).[e] Rate coefficients are estimated based on the analogous $Cl + C_3H_8$ reaction[46−48] divided by 4.0 to account for the kinetic isotope effect (as described in the experimental section). [f] Rate coefficients are estimated based on the analogous $Cl + C_3H_8$ reaction[46−48] divided by 1.5 to account for the kinetic isotope effect (as described in experimental section). [g] The branching fraction determined by Droege and Tully[114] has been fit to the function $\phi = -0.293 + 0.00286T - 3.47 \times 10^{-6}T^2 + 1.51 \times 10^{-9}T^3$. Rate coefficients are estimated based on the analogous $OH + C_3D_8$ reaction.[114] [h] Rate coefficients are calculated based on the recommendation of Atkinson et al.[75] and the kinetic isotope effect obtained from this work (i.e., 1.25).[i] Rate coefficients are taken from an experimental kinetic determination of the OD self-reaction.[103] [j] Branching ratio to form C_3D_7O estimated on the basis of the C_2D_5/O_2 system.[76] [k] Estimated on the basis of the mean of the i-$C_3D_7O_2$ and n-$C_3D_7O_2$ self-reaction rate coefficients. [l] Literature value of $C_2D_5O_2 + DO_2$ is used as an estimate of the rate coefficient.[77] [m] Estimated on the basis of $CF_3O_2 + OD$.[115] [m] Estimated on the basis of $C_2D_5OOD + O_2$.[29] [o] Estimated on the basis of i-$C_3D_7 + i$-$C_3D_7O_2$.[105] [p] Estimated on the basis of the CD_3/O_2 system.[79] [q] Estimated on the basis of $C_2D_5O + C_2D_5$.[80] [r] Calculated based on an average of three literature studies.[79,90,91] [s] Effective second-order rate coefficient is calculated from the expression given by DeMore et al.,[49] where $k_0^{300} = 1.2 \times 10^{-30}$ cm^6 $molecule^{-2}$ s^{-1}, $k_\infty^{300} = 1.4 \times 10^{-12}$ cm^3 $molecule^{-1}$ s^{-1}, $n = 3.0$, $m = 1.7$, and $F_{cent} = 0.46$. k_0^{300}, k_∞^{300}, and F_{cent} are taken from actual room temperature measurements of $CD_3 + O_2$.[92] The temperature dependence is estimated from the analogous $CH_3 + O_2$ reaction.[49] [t] Effective second-order rate coefficient is calculated from the expression given by DeMore et al.[49] where $k_0^{300} = 5.7 \times 10^{-32}$ cm^6 $molecule^{-2}$ s^{-1}, $k_\infty^{300} = 7.5 \times 10^{-11}$ cm^3 $molecule^{-1}$ s^{-1}, $n = 1.6$, $m = 0$, and $F_{cent} = 0.6$. [u] Estimated on the basis of $C_2D_5 + Cl$.[84] [v] Estimated on the basis of $C_2D_5O_2$+ Cl.[85] [w] Estimated on the basis of $Cl_2 + i$-C_3D_7.[86] [x] Pre-exponential factor, A, is taken from an absolute value measurement of the $D + Cl_2$ reaction,[93] and the temperature dependence is estimated from the analogous $H + Cl_2$ reaction.[94] [y] Rate coefficients are estimated based on the analogous $I + n$-C_3H_7I reaction[116] multiplied by 2.3, which is calculated based on the negative kinetic isotope effect measured for the $I + CH_3I/I + CD_3I$ reaction system.[96] [z] Estimated on the basis of $I + n$-C_3D_7I.[96,116] [aa] Estimated on the basis of $I + C_2D_5$.[97] [ab] Estimated on the basis of $I_2 + n$-C_3D_7.[89] [ac] Rate coefficients are estimated based on the analogous $HI + OH$ reaction[81] divided by 2.3, which is calculated based on the kinetic isotope effect measured for the HCl + OH/ DCl + OD reaction system.[98] [ad] Estimated on the basis of $DI + i$-C_3D_7.[99,100] [ae] Rate coefficients are estimated based on the analogous $HI + i$-C_3H_7 reaction[99] divided by 1.8, which is calculated based on the kinetic isotope effect measured for the HI + *tert*-C_4H_9/DI + *tert*-C_4H_9 reaction system.[100] [af] Rate coefficients are estimated based on the analogous decomposition of n-C_3H_7I[117] divided by 3.2, which is calculated based on the kinetic isotope effect measured for the CH_3I/CD_3I decomposition system.[102] [ag] Rate coefficients are estimated based on the analogous decomposition of i-C_3H_7I[118] divided by 3.2, which is calculated based on the kinetic isotope effect measured for the CH_3I/CD_3I decomposition system.[102]

elimination of HO_2 or DO_2 from the stabilized RO_2 radical and redissociation of the RO_2 to reactants followed by "prompt" HO_2 or DO_2 formation in a subsequent reactive encounter.[19,33,37,39] Both the "prompt" formation and the HO_2 elimination are substantially (2−3 times) slower for the deuterated isotopomers. The relative contributions of these pathways have been experimentally investigated by Kaiser[7] for $C_2H_5 + O_2$.

At the highest temperatures of the present experiments the rise of the "delayed" DO_2 (which is generated subsequent to stabilization of the alkylperoxy radical) becomes difficult to experimentally distinguish from the "prompt" DO_2 (which is formed from the initial chemically activated RO_2^* complex). As Miller and Klippenstein have previously discussed,[23] as the temperature is raised collisional stabilization of the peroxy radical becomes less effective, its thermal dissociation becomes faster, and the fraction of DO_2 molecules (or HO_2 molecules in the nondeuterated systems) generated by the direct reaction increases. This behavior can be discerned in the temperature

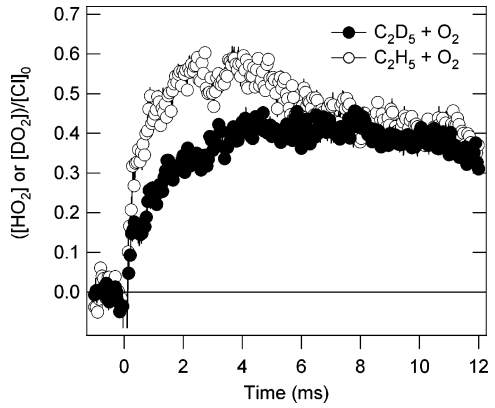

Figure 1. Comparison of DO_2 formation from Cl-initiated oxidation of C_2D_6 (solid circles) with HO_2 formation from C_2H_6 oxidation (open circles) at a temperature of 698 K and a total pressure of 61.5 Torr obtained by infrared FM spectroscopy. The experimental concentration is determined relative to the initial Cl atom concentration using the reference $Cl/CH_3OH/O_2$ system. There is no arbitrary scaling of the amplitudes.

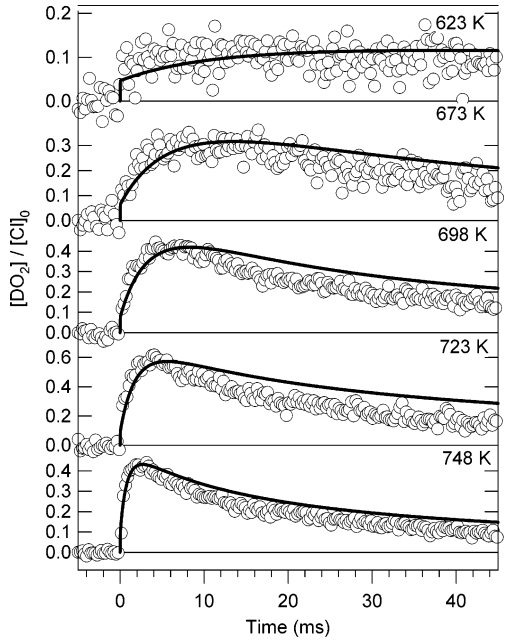

Figure 2. Comparison of the predicted (solid curves) and observed (open circles) DO_2 produced in the Cl-initiated oxidation of C_2D_6 at several temperatures and a total density of 8.45×10^{17} cm^{-3} obtained by infrared FM spectroscopy. The experimental concentration is determined relative to the initial Cl atom concentration using the reference $Cl/CH_3OH/O_2$ system. There is no arbitrary scaling of the amplitudes.

dependence of the individual rate coefficients in Table 1, for example; the direct reaction rate coefficient is nearly independent of temperature, but because the stabilization rate coefficient drops rapidly with increasing temperature, the fraction of DO_2 produced via the chemically activated channel increases at higher temperature. The rate constant for elimination of DO_2 from thermalized RO_2 radicals increases rapidly with increasing temperature, and at some temperature the "stabilization limit" is reached.[23] Above this temperature stabilization into the RO_2 well is impossible at any pressure. Beyond the stabilization limit, the "delayed" DO_2 is not merely experimentally indistinguishable from the "prompt" DO_2, but the distinction loses chemical meaning: essentially all products are formed "promptly" from the chemically activated species. Thus, in the high-temperature

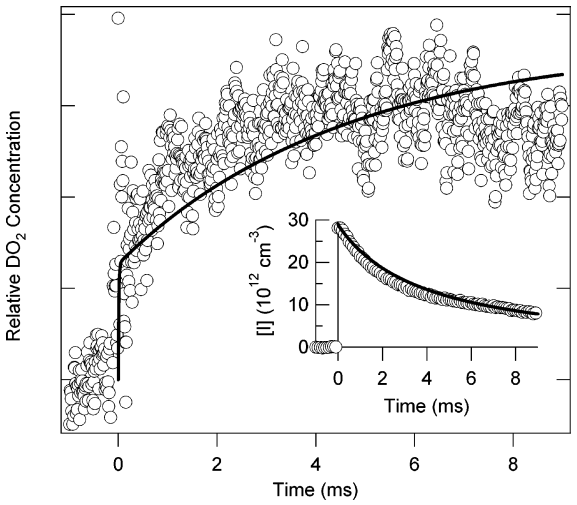

Figure 3. Comparison of the predicted (solid curve) and observed (open circles) DO_2 and I (shown as an inset) produced in the photodissociation of C_2H_5I at 673 K and 25 Torr obtained by infrared FM spectroscopy. Observed iodine atom concentrations are derived by using the absolute absorption cross section for the $F^* = 3 \leftarrow F = 4$ hyperfine transition of iodine atoms at 1.315 μm.[65,66]

regime (above ~750 K) direct, prompt DO_2 dominates the overall production of DO_2.

Figure 3 shows a comparison of the predicted and observed DO_2 and I signals at 673 K and 25 Torr in the $C_2D_5 + O_2$ experiments initiated by direct photolysis of C_2D_5I (the measured I atom concentration is shown as an inset). The agreement between the experimental data and the model is fairly good for DO_2 and reasonably good for I atoms although the model does not perfectly capture the time behavior of the I-atom decay. As shown in Table 4, the full kinetic model for the $C_2D_5 + O_2$ system consists of approximately 50 chemical reactions. However, the rise of the DO_2 signal, just as the rise of the HO_2 signal in the normal-abundance experiments, is primarily sensitive to $C_2D_5 + O_2$, the self-reactions of DO_2 and $C_2D_5O_2$, the cross-reactions of DO_2 and $C_2D_5O_2$, and the reactions of DO_2 and $C_2D_5O_2$ with I atoms. Unfortunately, the kinetics of the deuterated side chemistry reactions have hardly been experimentally studied at the temperatures of the current experiments, and thus, most of their rate coefficients are estimated based on reactions of the analogous nondeuterated species. Some uncertainties still remain as to the initial alkyl radical concentration. Because the photolysis of the alkyl iodides does not have a reference reaction like that of the Cl-initiated oxidation, the HO_2 (DO_2) signals are scaled relative to the observed initial I atom concentration. However, as postulated in a previous publication,[38] it is conceivable that enough excess energy remains in the alkyl radical after the 266 nm photolysis to dissociate some of the alkyl radicals before they are collisionally stabilized. Despite some unresolved issues,[38] the kinetic model does a very good job at describing both the prompt and delayed DO_2 formation corroborating the results from earlier work[23,38] that the theory of the ethyl radical with O_2 is very well established at this time.[40]

The next step is to look at the reaction of propyl radicals with O_2. Figures 4 and 5 show experimental DO_2 traces taken in the direct photolysis experiments of n-C_3D_7I and i-C_3D_7I at 673 K and 25 Torr. The time behavior of the DO_2 production is substantially different for the two propyl isomers, and this difference is more pronounced than the one observed in the analogous nondeuterated reactions.[38] DO_2 formation from i-$C_3D_7 + O_2$ displays a larger prompt yield and a faster secondary

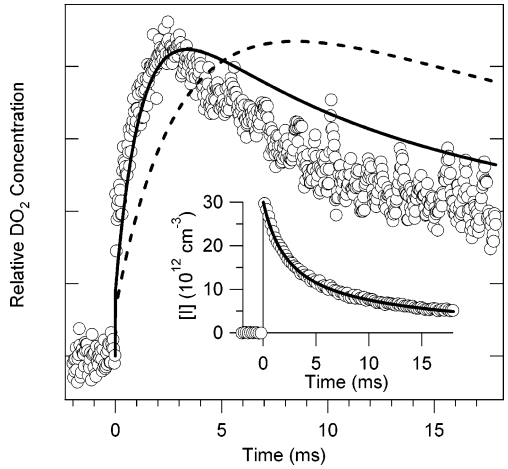

Figure 4. Comparison of the predicted (solid and dashed curves) and observed (open circles) DO_2 and I (shown as an inset) produced in the photodissociation of *i*-C_3D_7I at 673 K and 25 Torr obtained by infrared FM spectroscopy. The curves show the simulation results of the present model and the simulation results of the previous model.[38] Both models simulate the I-atom concentration almost identically, and thus, the simulation curves lie on top of each other. Observed iodine atom concentrations are derived by using the absolute absorption cross section for the $F^* = 3 \leftarrow F = 4$ hyperfine transition of iodine atoms at 1.315 μm.[65,66]

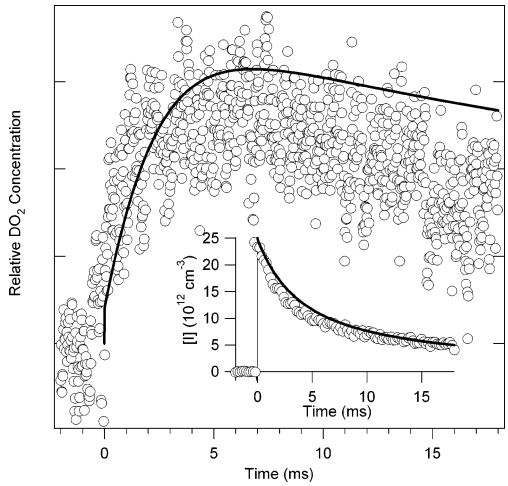

Figure 5. Comparison of the predicted and observed DO_2 and I (shown as an inset) produced in the photodissociation of *n*-C_3D_7I at 673 K and 25 Torr obtained by infrared FM spectroscopy. Observed iodine atom concentrations are derived by using the absolute absorption cross section for the $F^* = 3 \leftarrow F = 4$ hyperfine transition of iodine atoms at 1.315 μm.[65,66]

delayed production rate than those of the DO_2 formed from *n*-C_3D_7 + O_2; scaled to the initial I atom concentration, the peak DO_2 signal is approximately 3 times greater in the *i*-C_3D_7 + O_2 reaction than in the *n*-C_3D_7 + O_2 reaction. As discussed in a previous publication,[38] two main factors contribute to these differences: the energy of the transition state for DO_2 elimination is lower with respect to reactants in the isopropyl + O_2 reaction (-6.0 kcal mol^{-1} in isopropyl + O_2 vs -3.8 kcal mol^{-1} in *n*-propyl + O_2), and entropically, the elimination transition state of the isopropylperoxy radical is favored because there are six available D atoms in the two adjacent methyl groups in isopropylperoxy versus two adjacent D atoms in the case of *n*-propylperoxy radical.

Figure 4 shows a typical comparison of the predicted and observed DO_2 and I signals at 673 K and 25 Torr in the *i*-C_3D_7 + O_2 experiments initiated by direct photolysis of *i*-C_3D_7I (the

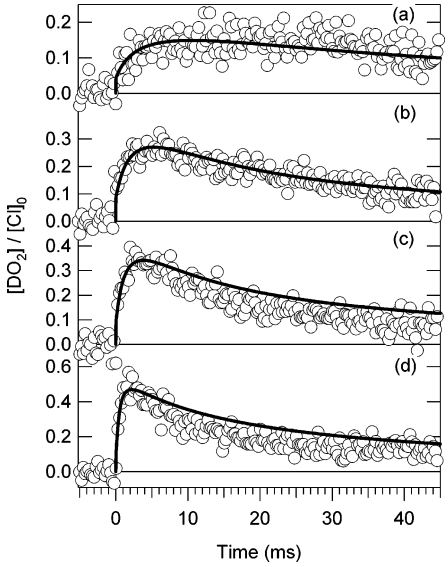

Figure 6. Comparison of the predicted (solid curves) and observed (open circles) DO_2 produced in the Cl-initiated oxidation of C_3D_8 at the following temperatures and pressures obtained by infrared FM spectroscopy: (a) 632 K and 45 Torr; (b) 648 K and 25 Torr; (c) 673 K and 25 Torr; and (d) 703 K and 60 Torr. The experimental concentration is determined relative to the initial Cl atom concentration using the reference $Cl/CH_3OH/O_2$ system. There is no arbitrary scaling of the amplitudes.

measured I atom concentration is shown as an inset) using the present and previously employed[38] kinetic models. The most significant difference between the two kinetic models is the somewhat different values for the rate coefficients for the elementary reaction steps involved in the isopropyl + O_2 reaction (as derived from solutions to master equations using the present stationary point energies). The present model reproduces the experimental trace much better than the previous model capturing very well the delayed DO_2 formation and doing a better job (within a factor of 2) at simulating the prompt DO_2 formation. As shown in the inset, the model also reproduces very well the I-atom concentration. Figure 5 shows the same comparison shown in Figure 4 but for a typical *n*-C_3D_7 + O_2 experiment initiated by direct photolysis of *n*-C_3D_7I (the measured I-atom concentration is shown as an inset). The agreement for both DO_2 and I signals is similar to that observed in the case of the analogous nondeuterated reaction.[38] Figure 6 shows the predicted and observed DO_2 signals at four different temperatures in the C_3D_7 + O_2 Cl-initiated experiments. As discussed in the experimental section, this is mostly an *i*-C_3D_7 + O_2 model because the kinetic isotope effect in the Cl + C_3D_8 results in about 70% *i*-C_3D_7 and about 30% *n*-C_3D_7. The agreement between the experimental data and the model confirms that the experimental data can be reproduced with the kinetic models even if the initiation chemistry (and, thus, the additional side chemistry) is different.

It is important to see how well the new revised kinetic model reproduces the experimental data obtained in the study of the *i*-C_3H_7 + O_2 reaction (using the revised stationary point energies compared to the energies employed in a previous publication)[38] and to discuss how well the new theoretical model compares with previous literature studies. Figures 7 and 8 show the predicted HO_2 and I signals at different temperatures compared to the experimental observations of the previous study of the *i*-C_3H_7 + O_2 reaction by Estupiñán et al.[38] The revised kinetic models improve the description of both HO_2 and I, capturing very closely the prompt yield and the secondary HO_2 formation, and reasonably modeling the decay of the HO_2 signal at longer

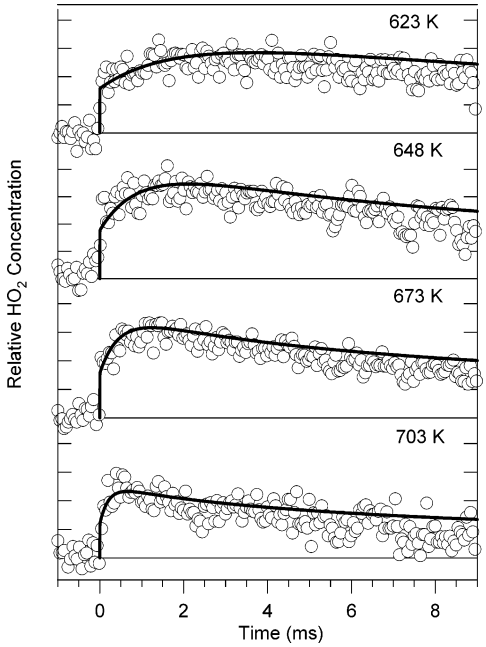

Figure 7. Comparison of the predicted (solid curves) and observed (open circles) HO_2 produced in the photodissociation of *i*-C_3H_7I at several temperatures and a total density of 3.65×10^{17} cm^{-3} obtained by infrared frequency modulation spectroscopy.

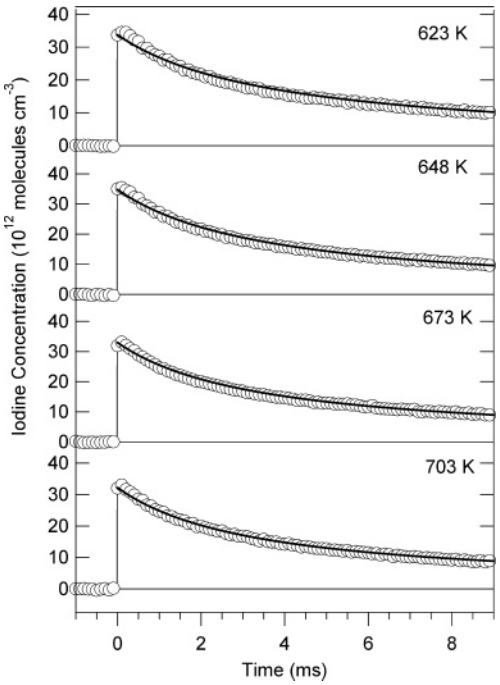

Figure 8. Comparison of the predicted (solid curves) and observed (open circles) I atom profiles produced in the photodissociation of *i*-C_3H_7I at several temperatures and total density of 3.65×10^{17} cm^{-3} obtained by infrared absorption spectroscopy. Observed iodine atom concentrations are derived by using the absolute absorption cross section for the $F^* = 3 \leftarrow F = 4$ hyperfine transition of iodine atoms at 1.315 μm.[65,66]

times (note that the time scale in these figures is different than that in Figure 2 and Figure 6). The previous model underestimated the prompt HO_2 production, especially as the temperature increased, and displayed slower secondary production rates than observed experimentally. The HO_2 production from the reaction of isopropyl radicals with O_2 appears well understood by the theory employed in this study, and it seems that the additional chemistry is adequately described by the kinetic models.

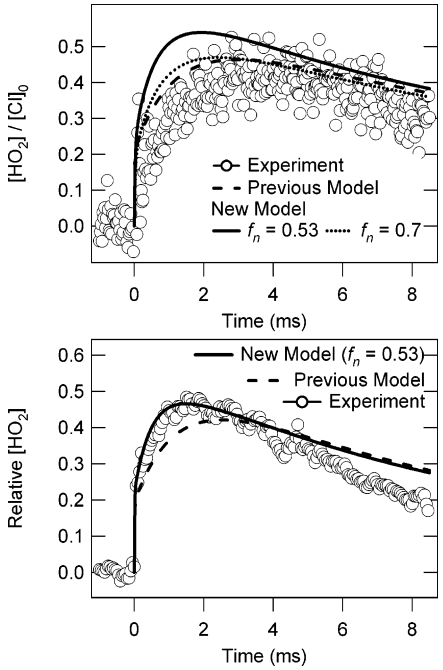

Figure 9. Comparison of predicted (solid curves) and observed (open circles) HO_2 produced in the Cl-initiated oxidation of C_3H_8 at 673 K for a total density of 8.45×10^{17} cm^{-3}, measured by infrared frequency modulation spectroscopy.[19,33] Also shown as a dashed curve for comparison is the predicted HO_2 generated by the previously employed kinetic model.[38] The dotted curve in (a) shows a model using the present stationary point energies and a larger branching to *n*-propyl in the reaction of Cl with propane. The measurement in (a) is obtained using Cl_2 photolysis as the Cl atom source, and the HO_2 concentration is determined relative to the initial Cl atom concentration using the reference $Cl/CH_3OH/O_2$ system. In (b) photodissociation of $(COCl)_2$ is used as the Cl atom source and no reference signal was measured; in this case the model and experiment are scaled to each other.

However, predictions for Cl-initiated C_3H_8 oxidation are worse with the present model. Figure 9a compares Cl-initiated C_3H_8 oxidation from photolysis of $Cl_2/O_2/C_3H_8$/He mixtures at 673 K to results of a model using the new values for isopropyl + O_2, assuming a branching between *n*-propyl and isopropyl formation in the Cl + C_3H_8 reaction of f_n = (*n*-propyl)/(*n*-propyl + isopropyl) = 0.53 based on extrapolation of lower-temperature measurements.[46−48] Figure 9a also shows a model where the *n*-propyl branching fraction is changed to 0.7, for which the agreement is slightly improved. It is possible that the branching favors *n*−propyl more than a simple extrapolation would predict. Furthermore, as shown in Figure 9b, modeling of new measurements using 266 nm photolysis of $(COCl)_2$ as an alternative source of Cl atom shows better agreement using the new stationary point energies than the old energies (leaving the *n*-propyl branching fraction unchanged at 0.53). Further investigation of the Cl-initiated propane oxidation, using various Cl-atom sources to change the competing and secondary chemistry, may be warranted.

As stated in the introduction, direct photolysis experiments permit lower O_2 concentrations to be employed in the experimental studies enabling measurements of the prompt rise time, a quantity that was not possible to measure in the Cl-initiated experiments. At high temperatures (where stabilization does not contribute) this quantity should be closely related to the overall reaction rate constant for R + O_2, although under the present conditions such a decomposition into elementary rate coefficients remains qualitative. Figure 10 shows a comparison of the experimental relative HO_2 concentration obtained by a typical *i*-C_3H_7 + O_2 experiment initiated by direct photolysis

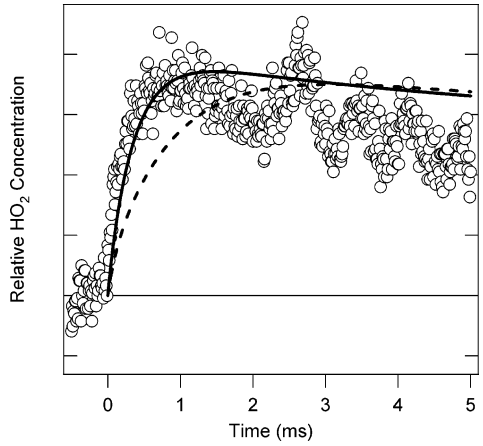

Figure 10. Comparison of the predicted (solid curve) and observed (open circles) HO_2 produced in the photodissociation of *i*-C_3H_7I at 673 K and 25 Torr and an O_2 concentration of 2.6×10^{15} cm^{-3} (factor of 60 lower in O_2 concentration than in most other experiments conducted in this study) obtained by infrared FM spectroscopy. The dashed curve is the predicted HO_2 generated by the previously employed kinetic model, shown for comparison.[38]

of *i*-C_3H_7I at a temperature of 703 K, a total density of 3.65×10^{17} cm^{-3}, and an O_2 concentration of 2.6×10^{15} cm^{-3}. The solid curve shows the simulation obtained using the present kinetic model and the dashed curve shows simulation obtained using the previous kinetic model.[38] The latest kinetic model reproduces the "resolved prompt rise time" to within about 25% and does a reasonable job at capturing the decay of the HO_2 signal. On the other hand, the "compromise model" substantially underestimates the HO_2 rise time. Similar agreement between theory and experiment was observed between the latest kinetic model and all the other relatively low O_2 experiments conducted in this work (i.e., O_2 concentrations ranging from 1.9×10^{15} cm^{-3} to 1.1×10^{16} cm^{-3}). Overall, a good level of agreement is found between theory and experiments over the entire range of O_2 concentrations considered in this work (i.e., 1.9×10^{15} cm^{-3} to 1.5×10^{17} cm^{-3}; a factor of about 80 in O_2 concentrations).

The next step is to verify how well the new revised theoretical model of *i*-$C_3H_7 + O_2$ agrees with literature studies because this is the oxidation reaction where revisions in the theory were performed with respect to previous work.[38] It is important to point out that the *i*-$C_3H_7 + O_2$ theoretical model presented in a previous work[38] was largely decided by trying to be as consistent with the literature measurements as possible and, at the same time, trying to simulate the new experimental observations as well as possible (i.e., a "compromise model"). A similar approach is taken in the present work, but the weighting given to the literature values is reinvestigated. Three pieces of information are available from the literature: the equilibration of *i*-C_3H_7 radicals with O_2 to form *i*-$C_3H_7O_2$ radicals, the room-temperature rate coefficient for *i*-$C_3H_7 + O_2$ to form products, and the high-temperature rate coefficients for *i*-$C_3H_7 + O_2$ to form propene.

Slagle and co-workers[8,42] studied the equilibration of isopropyl radicals with O_2 over a range of 100 K (i.e., 592−692 K) in the transition region by monitoring the decay of isopropyl radicals employing photoionization mass spectrometry. Figure 11 compares the results of the equilibrium constant derived by master-equation calculations using the present and previous theory[38] to the experimental values obtained by Slagle and coworkers[8,42] (error bars indicate the experimental uncertainty of ±60% estimated by Slagle et al.).[42] Both theoretical models of the equilibrium constant lie within the uncertainties calculated

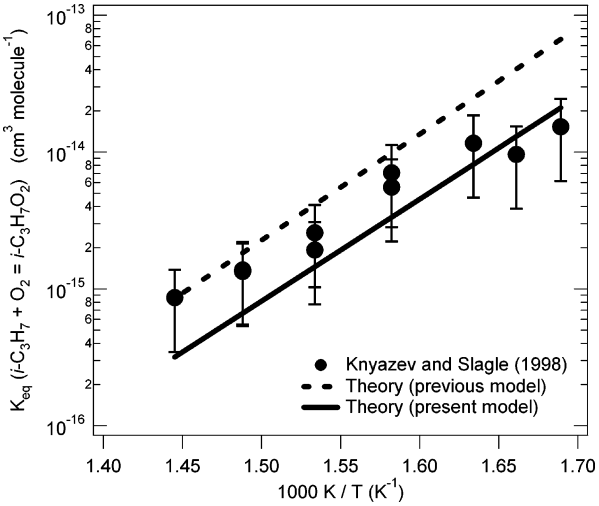

Figure 11. Comparison of the predicted (lines) and measured (solid circles) equilibrium constant for the reaction of *i*-$C_3H_7 + O_2$ to form *i*-$C_3H_7O_2$. The predicted equilibrium constants are derived from solutions to master equations and the measured equilibrium constant is taken from the work of Knyazev and Slagle[8] (error bars indicate the experimental uncertainty of ±60% estimated by Slagle et al.).[42] The solid curve shows the simulations results of the present model and the dashed curve shows the simulation results of the previous model.[38]

by Slagle et al.;[42] however, the agreement with the present theory is excellent at lower temperatures.

Ruiz and Bayes[73] measured the absolute rate coefficient of *i*-$C_3H_7 + O_2$ at room temperature by using direct monitoring of the radicals with photoionization mass spectrometry. Ruiz and Bayes[73] obtained the following rate coefficients: $(1.04 \pm 0.38) \times 10^{-11}$ at a pressure of 1 Torr and values ranging from $(1.37 \pm 0.64) \times 10^{-11}$ cm^3 $molecule^{-1}$ s^{-1} to $(1.61 \pm 0.34) \times 10^{-11}$ cm^3 $molecule^{-1}$ s^{-1} at a pressure of 4 Torr (different ionization chambers and radical precursors were employed in the higher pressure experiments). Within the experimental uncertainties, the measured rate coefficients are in very good agreement with the calculated values: 1.21×10^{-11} cm^3 $molecule^{-1}$ s^{-1} at 1 Torr and 1.73×10^{-11} cm^3 $molecule^{-1}$ s^{-1} at 4 Torr.

Gulati and Walker[43] measured propene and propane yields, by gas chromatography, formed in the oxidation of isobutyraldehyde (over the temperature range of 653−773 K and a pressure of 50 Torr), and the results were used to obtain rate coefficients for the *i*-$C_3H_7 + O_2$ reaction to form the propene product. Master-equation calculations performed at 653, 693, 733, and 773 K and a total pressure of 50 Torr have been compared with the results obtained by Gulati and Walker,[43] and it is found that the simulated rate coefficients are a factor of 6 higher than the values given by Gulati and Walker's[43] (i.e., a substantially larger difference than observed when comparing Gulati and Walker's[43] values with the results of the previous "compromise model").[38] Two observations can be made in regard to the study of Gulati and Walker:[43] the measured rate coefficients are derived by fitting the data to a complex kinetic mechanism and the study is inherently a relative rate determination. The accuracy of the results is therefore dependent on both the accuracy of the assumed kinetic mechanism and on the accuracy of the literature rate coefficients employed in the relative rate determination. The agreement between the kinetic models employed to simulate the experimental data presented in this work, particularly the prompt rise time measurements, and between the theoretical results and the literature studies reviewed here (other than the study presented by Gulati and

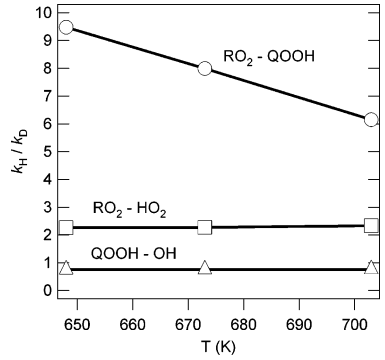

Figure 12. Deuterium kinetic isotope effect (k_H/k_D) as a function of temperature and a total density of 3.65×10^{17} cm^{-3} derived from solutions to master equations for 3 key elementary steps in the study of n-$C_3H_7 + O_2$.

Walker[43]) suggests that a reinvestigation of the high-temperature kinetics of the i-$C_3H_7 + O_2$ reaction is warranted.

Deuterium kinetic isotope effects resulting from comparing the calculated elementary rate coefficients (arising from solutions to time-dependent master equations) of the nondeuterated to the deuterated ethyl and propyl radicals with O_2 can be used to gain insight into the mechanism (i.e., in terms of expected H-atom motion). Figure 12 shows the calculated deuterium kinetic isotope effect (shown as k_H/k_D) for the reaction of n-$C_3H_7 + O_2$ for three temperatures (i.e., 648, 673, and 703 K) and a total density of 3.65×10^{17} cm^{-3} for three specific elementary reaction steps. The kinetic isotope effects for the analogous reaction steps in i-$C_3H_7 + O_2$ and in $C_2H_5 + O_2$ are similar. The circles show the isomerization step from $CH_3CH_2CH_2OO$ to CH_3CHCH_2OOH which occurs via a 5-membered ring transition state. This reaction step precedes the elimination of OH, which is the principal reaction pathway for OH formation, and it is the main formation step for QOOH species, which is related to chain branching in low-temperature hydrocarbon oxidation. The kinetic isotope effect for this reaction step ranges from 9.5 to 6.2 depending on the temperature. This is completely consistent with mainly H-atom motion as the H attached to the β-CH_2 group migrates toward the O-atom attached to the end of the RO_2 radical. The concomitant large change in frequency between reactants and transition state of vibrational modes involving this H atom implies that the zero-point energy difference between reactants and transition state will undergo a substantial decrease upon deuteration, increasing the effective energy barrier and reducing the rate coefficient.[44] The squares show the kinetic isotope effect for the concerted elimination of HO_2 from the RO_2 radical (i.e., $CH_3CH_2CH_2OO \rightarrow CH_3CHCH_2 + HO_2$). This is the principal reaction pathway for HO_2 formation. The kinetic isotope effect for this reaction step is about 2, a smaller kinetic isotope effect than calculated in the isomerization step suggesting less H-atom motion. Essentially, in the elimination step, the O-atom attached to the end of the RO_2 radical grabs the H-atom attached to the β-CH_2 group and then flies away with it, involving a fair amount of H-atom motion but less than in the isomerization step where the H migrates toward the O-atom. Third, the triangles show the kinetic isotope effect for elimination of OH from the QOOH species (i.e., $CH_3CHCH_2OOH \rightarrow CH_3CHCH_2O + OH$), the principal reaction pathway for OH formation. The kinetic isotope effect for this reaction step is about 0.8, a slightly inverse kinetic isotope effect. This step involves the rupture of an O−O bond, leading to little H-atom motion, which is consistent with a kinetic isotope effect around 1. It should finally be noted that, because of the effects of deuteration on collisional energy transfer, the overall kinetic isotope effects can be expected to exhibit a dependence on the total pressure.

Conclusions

Time-resolved production of HO_2 and DO_2 from the reactions of nondeuterated and deuterated ethyl and propyl radicals with O_2 have been measured as a function of temperature and pressure in the "transition region" between 623 and 748 K. Experimental measurements, using both pulsed-photolytic Cl-atom initiated oxidation of ethane and propane and direct photolysis of ethyl, *n*-propyl and isopropyl iodides, have been compared to kinetic models based on the results of time-dependent master equation calculations with *ab initio* characterization of stationary points. The present models accurately describe the time scale and amplitude of the DO_2 formation (or HO_2 formation in the nondeuterated reactions studies) from $C_2D_5 + O_2$, n-$C_3D_7 + O_2$, i-$C_3D_7 + O_2$, and i-$C_3H_7 + O_2$. Overall, a very good level of agreement is found between theory and experiments over a wide range of O_2 concentrations, temperatures and pressures. Direct photolysis experiments permitted lower O_2 concentrations to be employed in the experimental studies enabling measurements of the prompt rise time; a quantity that was not possible to measure in the Cl-initiated experiments because of side chemistry complications. Excellent agreement is found between previous literature studies and the theory presented in this work except in the case of the high-temperature rate coefficients measured by Gulati and Walker[43] for the reaction of i-$C_3H_7 + O_2$ to form propene. A reinvestigation of the high-temperature kinetics of the i-$C_3H_7 + O_2$ reaction is suggested. The results from the present work indicate that the theory for HO_2 formation in the reactions of ethyl and both isomeric forms of propyl radicals with O_2 are very well established at this time. As a result, this study forms the groundwork for the study and interpretation of larger and more complex $R + O_2$ systems. In addition, we have seen how deuterium kinetic isotope effects resulting from comparing the calculated elementary rate coefficients (arising from solutions to time-dependent master equations) of the nondeuterated to the deuterated ethyl and propyl radicals with O_2 can be used to gain insight on the accuracy of the theoretical picture (i.e., in terms of expected H-atom motion). Finally, this study forms the basis for future studies of partially deuterated species, which are expected to give site-specific information.

Acknowledgment. The experiments reported here were facilitated by the outstanding technical support of Leonard E. Jusinski. This work is supported by the Division of Chemical Sciences, Geosciences, and Biosciences, the Office of Basic Energy Sciences, the U.S. Department of Energy. The work at Argonne (S.J.K.) was supported under DOE Contract Number DE-AC02-06CH11357. Sandia is a multiprogram laboratory operated by Sandia Corporation, a Lockheed Martin Company, for the National Nuclear Security Administration under contract DE-AC04-94-AL85000.

References and Notes

(1) Wallington, T. J.; Nielsen, O. J. Peroxy Radicals and the Atmosphere. In *Peroxyl Radicals*; Alfassi, Z. B., Ed.; John Wiley & Sons: West Sussex, U.K., 1997; pp 457−482.

(2) Tyndall, G. S.; Cox, R. A.; Granier, C.; Lesclaux, R.; Moortgat, G. K.; Pilling, M. J.; Ravishankara, A. R.; Wallington, T. J. *J. Geophys. Res. D* **2001**, *106*, 12157.

(3) Atkinson, R. *Atmos. Environ.* **2000**, *34*, 2063.

(4) Pitz, W. J.; Westbrook, C. K. *Combust. Flame* **1986**, *63*, 113.

(5) Westbrook, C. K. *Proc. Combust. Inst.* **2000**, *28*, 1563.

(6) Clifford, E. P.; Farrell, J. T.; DeSain, J. D.; Taatjes, C. A. *J. Phys. Chem. A* **2000**, *104*, 11549.
(7) Kaiser, E. W. *J. Phys. Chem. A* **2002**, *106*, 1256.
(8) Knyazev, V. D.; Slagle, I. R. *J. Phys. Chem. A* **1998**, *102*, 1770.
(9) Slagle, I. R.; Ratajczak, E.; Gutman, D. *J. Phys. Chem.* **1986**, *90*, 402.
(10) Slagle, I. R.; Feng, Q.; Gutman, D. *J. Phys. Chem.* **1984**, *88*, 3648.
(11) Baldwin, R. R.; Pickering, I. A.; Walker, R. W. *J. Chem. Soc. Faraday Trans. I* **1980**, *76*, 2374.
(12) McAdam, K. G.; Walker, R. W. *J. Chem. Soc. Faraday Trans. 2* **1987**, *83*, 1509.
(13) Walker, R. W.; Morley, C. Basic Chemistry of Combustion. In *Low-Temperature Combustion and Autoignition*; Pilling, M. J., Ed.; Elsevier: Amsterdam, 1997; pp 1−124.
(14) Dobis, O.; Benson, S. W. *J. Am. Chem. Soc.* **1993**, *115*, 8798.
(15) Kaiser, E. W. *J. Phys. Chem.* **1995**, *99*, 707.
(16) Kaiser, E. W.; Lorkovic, I. M.; Wallington, T. J. *J. Phys. Chem.* **1990**, *94*, 3352.
(17) Kaiser, E. W.; Rimai, L.; Wallington, T. J. *J. Phys. Chem.* **1989**, *93*, 4094.
(18) Wagner, A. F.; Slagle, I. R.; Sarzynski, D.; Gutman, D. *J. Phys. Chem.* **1990**, *94*, 1853.
(19) DeSain, J. D.; Klippenstein, S. J.; Miller, J. A.; Taatjes, C. A. *J. Phys. Chem. A.* **2003**, *107*, 4415.
(20) Rienstra-Kiracofe, J. C.; Allen, W. D.; Schaefer, III, H. F. *J. Phys. Chem A.* **2000**, *104*, 9823.
(21) Ignatyev, I. S.; Xie, Y.; Allen, W. D.; Schaefer, III, H. F. *J. Chem. Phys.* **1997**, *107*, 141.
(22) Miller, J. A.; Klippenstein, S. J.; Robertson, S. H. *Proc. Combust. Inst.* **2000**, *28*, 1479.
(23) Miller, J. A.; Klippenstein, S. J. *Int. J. Chem. Kinet.* **2001**, *33*, 654.
(24) Stark, M. S. *J. Am. Chem. Soc.* **2000**, *122*, 4162.
(25) Quelch, G. E.; Gallo, M. M.; Schaefer, III, H. F. *J. Am. Chem. Soc.* **1992**, *114*, 8239.
(26) Quelch, G. E.; Gallo, M. M.; Shen, M.; Xie, Y.; Schaefer, H. F., III; Moncrief, D. *J. Am. Chem. Soc.* **1994**, *116*, 4953.
(27) Chen, C. J.; Bozzelli, J. W. *J. Phys. Chem. A* **2000**, *104*, 9715.
(28) Bozzelli, J. W.; Dean, A. M. *J. Phys. Chem.* **1990**, *94*, 3313.
(29) Bozzelli, J. W.; Sheng, C. *J. Phys. Chem. A* **2002**, *106*, 1113.
(30) Sheng, C. Y.; Bozzelli, J. W.; Dean, A. M.; Chang, A. Y. *J. Phys. Chem. A* **2002**, *106*, 7276.
(31) Cullis, C. F.; Fish, A.; Saeed, M.; Trimm, D. L. *Proc. Roy. Soc. London Ser. A* **1966**, *289*, 402.
(32) Cullis, C. F.; Saeed, M.; Trimm, D. L. *Proc. Roy. Soc. London Ser. A* **1967**, *300*, 455.
(33) DeSain, J. D.; Clifford, E. P.; Taatjes, C. A. *J. Phys. Chem. A.* **2001**, *105*, 3205.
(34) DeSain, J. D.; Klippenstein, S. J.; Taatjes, C. A.; Hurley, M. D.; Wallington, T. J. *J. Phys. Chem. A* **2003**, *107*, 1992.
(35) DeSain, J. D.; Klippenstein, S. J.; Taatjes, C. A. *Phys. Chem. Chem. Phys.* **2003**, *5*, 1584.
(36) DeSain, J. D.; Taatjes, C. A. *J. Phys. Chem. A* **2001**, *105*, 6646.
(37) DeSain, J. D.; Taatjes, C. A.; Miller, J. A.; Klippenstein, S. J.; Hahn, D. K. *Faraday Discuss.* **2001**, *119*, 101.
(38) Estupiñán, E. G.; Klippenstein, S. J.; Taatjes, C. A. *J. Phys. Chem. B.* **2005**, *109*, 8374.
(39) Taatjes, C. A. *J. Phys. Chem. A* **2006**, *110*, 4299.
(40) Carstensen, H.-H.; Naik, C. V.; Dean, A. M. *J. Phys. Chem. A* **2005**, *109*, 2264.
(41) Kaiser, E. W. *J. Phys. Chem. A* **1998**, *102*, 5903.
(42) Slagle, I. R.; Ratajczak, E.; Heaven, M. C.; Gutman, D.; Wagner, A. F. *J. Am. Chem. Soc* **1985**, *107*, 1838.
(43) Gulati, S. K.; Walker, R. W. *J. Chem. Soc. Faraday Trans. 2* **1988**, *84*, 401.
(44) Melander, L.; Saunders Jr., W. H. *Reaction Rates of Isotopic Molecules*; John Wiley and Sons: New York, 1980.
(45) Berkowitz, J.; Ellison, G. B.; Gutman, D. *J. Phys. Chem.* **1994**, *98*, 2744.
(46) Sarzynski, D.; Sztuba, B. *Int. J. Chem. Kinet.* **2002**, *34*, 651.
(47) Tschuikow-Roux, E.; Niedzielski, J.; Faraji, F. *Can. J. Chem.* **1985**, *63*, 1093.
(48) Taatjes, C. A., Unpublished results. Measurements of rate coefficients and HCl yields from reactions of Cl with partially deuterated propanes suggest an *n*-propyl branching fraction of 0.53 ± 0.16 at 575 K.
(49) DeMore, W. B.; Sander, S. P.; Golden, D. M.; Hampson, R. F.; Kurylo, M. J.; Howard, C. J.; Ravishankara, A. R.; Kolb, C. E.; Molina, M. J. *Chemical Kinetics and Photochemical Data for Use in Stratospheric Modeling*; Jet Propulsion Laboratory: Pasadena, CA, 1997.
(50) Fink, E. H.; Ramsay, D. A. *J. Molec. Spectrosc.* **2002**, *216*, 322.
(51) Pine, A. S. *J. Opt. Soc. Am.* **1976**, *66*, 97.
(52) McIlroy, A.; Nesbitt, D. J. *Chem. Phys. Lett.* **1991**, *187*, 215.
(53) Pilgrim, J. S.; Jennings, R. T.; Taatjes, C. A. *Rev. Sci. Instrum.* **1997**, *68*, 1875.
(54) Bjorklund, G. C. *Opt. Lett.* **1980**, *5*, 15.
(55) Hall, G. E.; North, S. *Annu. Rev. Phys. Chem.* **2000**, *51*, 243.
(56) Taatjes, C. A.; Oh, D. B. *Appl. Opt.* **1997**, *36*, 5817.
(57) Fink, E. H.; Ramsay, D. A. *J. Mol. Spectrosc.* **1997**, *185*, 304.
(58) Becker, K. H.; Fink, E. H.; Langen, P.; Schurath, U. *J. Chem. Phys.* **1974**, *60*, 4623.
(59) Hunziker, H. E.; Wendt, H. R. *J. Chem. Phys.* **1974**, *60*, 4622.
(60) Johnson, T. J.; Wienhold, F. G.; Burrows, J. P.; Harris, G. W.; Burkhard, H. *J. Phys. Chem.* **1991**, *95*, 6499.
(61) Burde, D.; McFarlane, R. *J. Chem. Phys.* **1976**, *64*, 1850.
(62) Burrows, M. *J. Chem. Phys.* **1984**, *81*, 3546.
(63) Donovan, R. J.; Husain, D. *Chem. Rev.* **1970**, *70*, 489.
(64) Young, A.; Houston, P. *J. Chem. Phys.* **1983**, *78*, 2317.
(65) Ha, T.-K.; He, Y.; Pochert, J.; Quack, M.; Ranz, R.; Seyfang, G.; Thanopoulos, I. *Ber. Bunsenges. Phys. Chem.* **1995**, *99*, 384.
(66) Davis, S.; Mulhall, P.; Bachman, M.; Kessler, W.; Keating, P. *J. Phys. Chem. A.* **2002**, *106*, 8323.
(67) Klippenstein, S. J.; Miller, J. A. *J. Phys. Chem A* **2002**, *106*, 9267.
(68) Sander, S. P.; Peterson, M.; Watson, R. T.; Patrick, R. *J. Phys. Chem.* **1982**, *86*, 1236.
(69) Hamilton, E. J.; Lii, R.-R. *Int. J. Chem. Kinet.* **1977**, *9*, 875.
(70) Dane, C. B.; Lander, D. R.; Curl, R. F.; Tittel, F. K.; Guo, Y.; Ochsner, M. I. F.; Moore, C. B. *J. Chem. Phys.* **1988**, *88*, 2121.
(71) Kircher, C. C.; Sander, S. P. *J. Phys. Chem.* **1984**, *88*, 2082.
(72) Fahr, A.; Laufer, A. H. *Int. J. Chem. Kinet.* **1993**, *25*, 1029.
(73) Ruiz, R. P.; Bayes, K. D. *J. Phys. Chem.* **1984**, *88*, 2592.
(74) Pilgrim, J. S.; McIlroy, A.; Taatjes, C. A. *J. Phys. Chem. A* **1997**, *101*, 1873.
(75) Atkinson, R.; Baulch, D. L.; Cox, R. A.; Hampson, R. F., Jr.; Kerr, J. A.; Rossi, M. J.; Troe, J. *J. Phys. Chem. Ref. Data* **1997**, *26*, 521.
(76) Wallington, T. J.; Dagaut, P.; Kurylo, M. J. *Chem. Rev.* **1992**, *92*, 667.
(77) Maricq, M. M.; Szente, J. J. *J. Phys. Chem.* **1994**, *98*, 2078.
(78) Atkinson, D. B.; Hudgens, J. W. *J. Phys. Chem. A* **1997**, *101*, 3901.
(79) Tsang, W.; Hampson, R. F. *J. Phys. Chem. Ref. Data* **1986**, *15*, 1087.
(80) Foucaut, J.-F.; Martin, R. *J. Chim. Phys.* **1978**, *75*, 132.
(81) Atkinson, R.; Baulch, D. L.; Cox, R. A.; Crowley, J. N.; Hampson, R. F., Jr.; Kerr, J. A.; Rossi, M. J.; Troe, J. *Summary of Evaluated Kinetic and Photochemical Data for Atmospheric Chemistry*, Nov 2003 ed.; IUPAC subcommittee on gas kinetic data evaluation for atmospheric chemistry; IUPAC: 2003.
(82) Hoyermann, K.; Olzmann, M.; Seeba, J.; Viskolcz, B. *J. Phys. Chem. A* **1999**, *103*, 5692.
(83) Atkinson, R. *Int. J. Chem. Kinet.* **1997**, *29*, 99.
(84) Maricq, M. M.; Szente, J. J.; Kaiser, E. W. *J. Phys. Chem.* **1993**, *97*, 7970.
(85) Maricq, M. M.; Szente, J. J.; Kaiser, E. W.; Shi, J. *J. Phys. Chem.* **1994**, *98*, 2083.
(86) Timonen, R. *Ann. Acad. Sci. Fenn. Ser. A2* **1988**, *218*, 5.
(87) Baulch, D. L.; Duxbury, J.; Grant, S. J.; Montague, D. C. *J. Phys. Chem. Ref. Data* **1981**, *10*, Supplement 1.
(88) Jenkin, M. E.; Cox, R. A.; Mellouki, A.; LeBras, G.; Poulet, G. *J. Phys. Chem.* **1990**, *94*, 2927.
(89) Hayes, D. M.; Strong, R. L. *J. Phys. Chem.* **1986**, *90*, 6305.
(90) Hassinen, E.; Koskikallio, J. *Acta Chem. Scand. Ser. A* **1979**, *33*, 625.
(91) Yee Quee, M. J.; Thynne, J. C. J. *Ber. Bunsenges. Phys. Chem.* **1968**, *72*, 211.
(92) Kaiser, E. W. *J. Phys. Chem.* **1993**, *97*, 11681.
(93) Jaffe, S.; Clyne, M. A. A. *J. Chem. Soc. Faraday Trans. 2* **1981**, *77*, 531.
(94) Berho, F.; Rayez, M.; Lesclaux, R. *J. Phys. Chem. A* **1999**, *103*, 5501.
(95) Hartley, D. B.; Benson, S. W. *J. Phys. Chem.* **1963**, *39*, 132.
(96) Skorobogatov, G. A.; Dymov, B. P.; Nedozrelova, I. V. *Zh. Org. Khim.* **1994**, *64*, 956.
(97) Hunter, T. F.; Kristjansson, K. S. *J. Chem. Soc. Faraday Trans. 2* **1982**, *78*, 2067.
(98) Warth, V.; Stef, N.; Glaude, P. A.; Battin-Leclerc, F.; Scacchi, G.; Côme, G. M. *Combust. Flame* **1998**, *114*, 81.
(99) Seetula, J. A.; Russell, J. J.; Gutman, D. *J. Am. Chem. Soc.* **1990**, *112*, 1347.
(100) Rossi, M. J.; Golden, D. M. *Int. J. Chem. Kinet.* **1983**, *15*, 1283.
(101) Yang, J. H.; Conway, D. C. *J. Chem. Phys.* **1965**, *43*, 1296.
(102) Kodama, S.; Ooi, Y. *Bull. Chem. Soc. Jpn.* **1990**, *63*, 877.
(103) Bedjanian, Y.; Laverdet, G.; LeBras, G. *J. Phys. Chem. A* **1998**, *102*, 953.
(104) Tsang, W. *J. Phys. Chem. Ref. Data* **1988**, *17*, 887.
(105) Munk, J.; Pagsberg, P.; Ratajczak, E.; Sillesen, A. *Chem. Phys. Lett.* **1986**, *132*, 417.
(106) Fittschen, C.; Frenzel, A.; Imrik, K.; Devolder, P. *Int. J. Chem. Kinet.* **1999**, *31*, 860.

(107) Batt, L. *Int. J. Chem. Kinet.* **1979**, *11*, 977.
(108) Choo, K. Y.; Benson, S. W. *Int. J. Chem. Kinet.* **1981**, *13*, 833.
(109) Kerr, J. A.; Trotman-Dickenson, A. F. *Trans. Faraday Soc.* **1959**, *55*, 572.
(110) Bencsura, Á.; Knyazev, V. D.; Xing, S.-B.; Slagle, I. R.; Gutman, D. *Proc. Combust. Inst.* **1992**, *24*, 629.
(111) Seakins, P. W.; Robertson, S. H.; Pilling, M. J.; Slagle, I. R.; Gmurczyk, G. W.; Bencsura, A.; Gutman, D.; Tsang, W. *J. Phys. Chem.* **1993**, *97*, 4450.
(112) Kerr, J. A.; Trotman-Dickenson, A. F. *Trans. Faraday Soc.* **1959**, *55*, 921.
(113) Daele, V.; Laverdet, G.; Poulet, G. *Int. J. Chem. Kinet.* **1996**, *28*, 589.
(114) Droege, A. T.; Tully, F. P. *J. Phys. Chem.* **1986**, *90*, 1949.
(115) Biggs, P.; Canosa-Mas, C. E.; Shallcross, D. E.; Vipond, A.; Wayne, R. P. *J. Chem. Soc. Faraday Trans.* **1997**, *93*, 2701.
(116) Sullivan, J. H. *J. Phys. Chem.* **1961**, *65*, 722.
(117) Butler, E. T.; Polanyi, M. *Trans. Faraday Soc.* **1943**, *39*, 19.
(118) Tsang, W. *J. Phys. Chem.* **1964**, *41*, 2487.